Express Polymer Letters Vol.16, No.6 (2022) 624–648
Available online at www.expresspolymlett.com
https://doi.org/10.3144/expresspolymlett.2022.46

Research article

Adsorption of estrogenic hormones in aqueous solution using electrospun nanofibers from waste cigarette butts: Kinetics, mechanism, and reusability

Muhammad Yasir[*], *Tomáš Šopík*, *Rahul Patwa*, *Dušan Kimmer*, *Vladimír Sedlařík*

Centre of Polymer Systems, University Institute, Tomas Bata University in Zlín, Třída Tomáše Bati 5678, 76001 Zlín, Czech Republic

Received 9 December 2021; accepted in revised form 14 February 2022

Abstract. This study emphasizes rapid and simultaneous adsorptive removal of estrogenic hormones (EH): estrone (E1), estradiol (E2), ethinylestradiol (EE2), and estriol (E3) from wastewater using recycled waste cigarette electrospun fibers (WCENFs). The submicron fibers exhibited a strong affinity towards all EH due to abundant hydrogen bonding interactions. The adsorption kinetics pseudo-first-order, pseudo-second-order, intra-particle diffusion, Elovich, and fractional power models were explored and fitted towards optimum conditions for the large-scale removal process of the EH. Results showed that E1, E2, and EE2 followed pseudo-second-order kinetics while E3 followed the pseudo-first-order kinetic model. In combination, the total adsorption capacity achieved was 2.14 mg/g, whereas the individual values for E1, E2, EE2, and E3 were 0.551, 0.532, 0.687, and 0.369 mg/g, respectively. The percentage efficiency of WCENFs was highest with EE2 ~64.3% and least with E3 ~34.6%. The WCENFs could repeatedly be used for four adsorption-desorption cycles as an effective adsorbent for the simultaneous removal of four EH via batch adsorption studies. According to the results obtained, the repurposing of waste cigarette butts to WCENFs presented itself as a suitable alternative for removing EH and possibly other organic pollutants from water.

Keywords: *industrial application, water treatment, estrogens removal, adsorption kinetics*

1. Introduction

Reportedly, over 5.5 trillion cigarettes are produced a year globally, with 4.5 trillion waste cigarette butts (CBs) causing approximately 2 million tons of littered butts a year without proper disposal [1, 2]. Cigarette smoking not only causes significant health damage to the smoker but also to the passive smoker, ultimately leading to continuous air pollution. The open disposal of CB in public areas such as bus stops, stations, parks, and gardens pollutes soil and water [3]. It degrades the chemical, physical and biological conditions of nature [1, 4]. The available cigarette in the market consists of 95% cellulose acetate (CA) [5]; the remaining are paper, polyvinyl alcohol, and tobacco. CB is approximately 30% in length and contains monofilament tow of CA combined with some additives and chemicals. The accumulation of traces of tobacco in these CBs and their disposal as wastes is a severe issue and a major threat to the ecosystem since they are non-degradable. These CB wastes are flushed away by rain drained into rivers, seas, and further into the oceans, which is devastating for marine life [6] as the contaminants of CBs are likely to enter the food chain. It is considered one of the most critical waste due to its high dispersion worldwide, causing severe health effects on the lives of humans [7]. Thus, it is necessary to identify a new method of recycling and repurposing CBs to counter this inevitable waste [8].

[*]Corresponding author, e-mail: yasir@utb.cz

Estrogenic hormones (EH) include estrone (E1), estradiol (E2), ethinylestradiol (EE2), and estriol (E3), also called endocrine-disrupting chemicals (EDCs), have adverse effects on humans and wildlife [9]. Residual of these micropollutants are present in micro and nanograms concentrations in local cleaning reservoirs of wastewater treatment [9]. In general, these EH (natural and synthetic) are majorly from anthropogenic sources, antibiotics, contraceptive pills, chemotherapy drugs and are present in excreting of humans and animals (feces and urine). These EH are released into the environment (*e.g.*, reservoirs, rivers, and lakes) via insufficiently treated effluents [10, 11]. For example, EH in the range of 3.4–41 ng/l has been reported in constructed wetlands of the Czech Republic [12]. At such high concentrations, they may harm the reproduction tendency of aquatic species and interrupt natural body hormones' function [13]. Studies have shown an increase in fish femininity, testicles weight loss in quails, and fertility disorder in alligators, which are a few of the many side effects [14]. Furthermore, a decline in male sperm count high breast and ovarian cancer risks in humans have been reported [15]. Amongst all EH, EE2 is the most dangerous due to its partial degradation, while its treatment and inadequate removal lead to colossal estrogenicity [16]. This issue has aroused deep concerns in the scientific world because these synthetic EH can interfere with functional groups of hormones synthesized naturally inside the body by mimicking them [17–21]. Thus, the presence of these EH is a severe threat to both human and aquatic life based on the source of food or drinking water [13, 21]. Hence, the EH require proper concurrent disposal and elimination from wastewater.

The conventional wastewater treatment plants cannot properly remove these hormones with low molecular weight and low biodegradability because they are difficult to be detected and quantified at extremely low concentrations [22]. Reportedly, various treatments have been applied, such as ozonation, membrane bioreactors, advanced oxidation, membrane filtration, photocatalytic degradation, and coagulation-flocculation, to counter this issue [23–25]. Each technique has some limitations, such as complexity, low efficiency, and by-products generated during the procedure require further sophisticated purification steps. Nano-filtration and reverse osmosis have also emerged as interesting methods, but the intense energy requirements make them unfeasible for selection [26, 27]. Adsorption is one such promising technique that has been found to address the issue of EH removal.

In addition to the sorption technique, the sorbent material is the most important and dominant factor. Several adsorbents have been reported for EH removal in previous studies, such as granules of activated charcoal [28, 29], fullerene [30, 31], carbon nanotubes [32], chitosan, activated carbon, chitin, multi-walled carbon nanotubes, carbon-based adsorbents prepared from industrial waste [33, 34], and activated carbon fibers modified with iron hydroxide [35]. All these materials in particles form are efficient in adsorbing EH when dispersed in solution due to the large surface area. Hence, they require modification and a further operable filtration technique after adsorption from wastewater, which increases the overall cost. Recently, submicron fibers as sorbents have an emerging interest because of their characteristic features such as lightweight, small fiber diameter, small pore size, high aspect ratio, and large specific surface area of fibers providing a greater contact of the solution with the adsorbent to significantly raise the filtration efficiency [36, 37]. In addition, this class of materials has been proven as suitable adsorbents to eradicate the subsequent additional separation step [38, 39]. Thus, the research essentially needs a new high-performance material specifically with an optimum disposal process efficiency. In the context of recycling materials, electrospinning is a versatile technique for generating a continuous fiber sheet with a diameter from tens to hundreds of nanometres for sophisticated solar cells, air purification, and water filtration techniques [40]. Moreover, electrospun polymers have proven to be an excellent choice for removing heavy metal ions, organic pollutants, and dyes from wastewater and have been used in wound healing, orthopedic and anti-bacterial applications [41–44]. Therefore, taking both aspects of recycling and removing organic molecules by efficient use of repurposed waste CBs will keep the environment clean and be an excellent solution to reduce micropollutants from wastewater. Presently, few studies have been done with CBs in different applications such as asphalt production, biofilm carrier, metal corrosion inhibitors [1], insecticides, fired clay brick filler [6], energy storage devices, and removal of bisphenol-A from wastewater [8]. However, modification of the CBs into spun fibers [45] will improve the adsorption efficiency of these materials due to

readily available functional groups (C=O, C–O–C, and C–O–H) to form hydrogen bonding with organic pollutants such as EH [8, 46]. So far, the adsorption of EH, to the best of our knowledge, has been explored to a lesser extent. Recently, few studies on the removal of different EH hormones by polyamide (PA) fibers, polyethersulfone (PES), and polyvinylidene (PVDF) membrane modified with polyvinyl pyrrolidone and titanium dioxide have been reported [9, 13, 47–49]. These studies were restricted to the filtration of single hormones. In our previous study, we reported the use of polyurethane (PU), cellulose acetate (CA), polyacrylonitrile (PAN), PA, and PES fibers for adsorption removal of different EH [50]. Hence, it is necessary to fill this gap by developing fibers produced from recycling CBs at optimum conditions with achieved desired least fiber diameter, thereby increasing surface area making the material an ideal candidate for the simultaneous removal of different EH. This process will not only reduce litter waste created from CBs, but it is a less costly method owing to the electrospinning technique, which requires less energy for the fabrication of fibers [51].

Herein, this paper aims to prepare waste cigarette electrospun nanofibers (WCENFs) for the batch adsorption of four EH (E1, E2, E3, and EE2). The prepared fibers are based on small fiber diameter formation to achieve high surface area and aspect ratio, thereby creating more sites available for adsorption. The objective is to focus on single and simultaneous adsorption of various EH in a one-step process. Further, to investigate the feasibility of the results using the experimental data, adsorption capacity and apply different kinetic models such as pseudo-first-order, pseudo-second-order, intraparticle diffusion, Elovich, and fractional power models were evaluated. These models help to understand the characteristics of adsorption kinetics that are essential for the selection of optimum conditions for the large-scale removal application of EH. The study also includes establishing the fibers' adsorption mechanism to understand interactions between WCENFs and EH. Then, the reusability in several adsorption-desorption cycles to assess the reliable effectiveness of this material. Finally, a comparative study on the instant adsorption efficiency of prepared PET/WCENFs (polyethylene terephthalate) syringe film against commercially available CA syringe film was analyzed.

2. Materials and methods

2.1. Materials and reagents

The CBs, regardless of brand, were collected over a week from the cigarette waste bins of Centre of Polymer Systems (CPS), Tomas Bata University in Zlin, Czech Republic. Four EH *viz*. estrone (E1) ≥99%, 17β-estradiol (E2) ≥98%, estriol (E3) ≥97%, and 17α-ethinylestradiol (EE2) ≥98% were purchased from Sigma-Aldrich Chemie GmbH, Germany. Butylated hydroxytoluene (BHT) and Swinnex film holders with Luer lock (25 mm diameter) were purchased from Sigma-Aldrich, Germany. Tetrahydrofuran (THF) were obtained from Carl Roth Rotisolv® HPLC (Karlsruhe, Germany). Acetonitrile (HPLC grade) and ethanol (HPLC grade >99% pure) were purchased from Honeywell and VWR, Czech Republic, respectively. Furthermore, sodium tetra-borate decahydrate (borax), citric acid, acetic acid (99%), and formic acid (98%) were purchased from PENTA s.r.o., the Czech Republic, and *N*,*N*-dimethylformamide (DMF >99.5%) from Lach-Ner, s.r.o., Czech Republic. Polyethylene oxide (PEO) from Scientific Polymer Products, Inc., Ontario, the USA. Deionized water (18.3 MΩ/cm, pH 7.3) was sourced from a Milli-Q ultra-pure (type 1) water purification system, Biopak® Polisher, Merck, the USA, and was used throughout the study.

2.2. Submicron-fibers fabrication

CBs were washed twice with distilled water to remove unwanted debris dust and dried in a hot-air oven for 6 h at 80 °C. Further, they were washed with ethanol and kept at 40 °C for 4 h. A total of 8 wt% of CBs were dissolved in a binary solution of acetic acid and formic acid in a ratio (2:1) to make a total solution of 400 g. Then, 3 wt% of PEO of the amount of the CBs was added for stability of the mixture to improve the structural properties of fibers. Finally, the mixture was stirred for 5 h at 400 rpm in a mechanical stirrer (Heidolph, RZR 2041). Electrical conductivity was adjusted to about 88.1 μS/cm by using a solution of borax and citric acid (BC) in a ratio (1:3), prior to electrospinning; this solution was prepared by dissolving 35 wt% of BC in DMF solution and stirring for 5 h at 400 rpm on a magnetic stirrer and viscosity of the solution during the preparation was kept at 0.95 Pa·s.

The electrospinning process was performed by nano spider technology using the NS Lab 200S equipment

(Elmarco, Czech Republic) to produce WCENFs on a polypropylene (PP) spun-bond non-woven sheet with a width of 40 cm. The applied supply was 75 kV, solution coming out of the bath to be sprayed from cord strings was set at 0.34 ml/min. The distance between the electrodes was 18 cm, the rotational speed of collecting fiber sheet fabric was 10 cm/min, and the temperature was 27±1 °C with the relative air humidity <35%. The solution properties were optimized before the electrospinning process, and the properties of the WCENFs are shown in Table 1.

The table shows the optimized properties of the polymer solution prepared from CBs for electrospinning and the average area mass of produced electrospun fibers. The aim of optimizing these parameters was to prepare the least diameter, defect-free, and beadles submicron fibrous mats from waste CBs.

2.3. Characterization

Morphological analysis was carried out using Nova 450 scanning electron microscope (SEM) (FEI, Thermo Fisher Scientific, USA) at 5-10 kV applied potential using a through-the-lens detector (TLD). It was done to observe the fiber surface morphology, the diameter size of fibers, and the defects in the structures such as beads. The software ImageJ version 1.52a was used to determine the average fiber diameter of samples.

X-ray diffractogram (XRD) of WCENFs was recorded using Miniflex™ 600 X-ray diffractometer (Rigaku, Japan), having CoK_β ($\lambda = 1.79$ Å) as a source. The angle 2θ was in the range from 5–90° with operating current, step size, step time, and operational voltage set to 15 mA, 0.02°, 10°/s, and 40 kV, respectively. The diffractograms obtained using Co source were converted to Cu using PowerDLL software converter 2.93 to compare data in the prior art.

To determine the functional groups present in WCENFs used for the adsorption of EH, Nicolet 320 Fourier transformed infrared spectroscopy (FTIR) (ThermoScientific, USA) equipped with Ge crystal was used. The attenuated total reflectance (ATR) spectra were recorded from 400–4000 cm^{-1} at ambient temperature with a scan rate of 16 and a resolution of 4 cm^{-1}.

The surface area analysis of WCENFs was made utilizing the Brunauer-Emmett-Teller (BET) high precision surface area and pore size analyzer BELSORP-mini II (BEL Japan, Inc., Japan) to determine the specific surface area. The substrate's outgassing was done at 100 °C for 12 h under vacuum before starting measurement. Air permeability and pore size distribution of submicron structure were assessed by flow porometer according to ASTM F316-03 (2011). Galpor (Porometer NV, Belgium) was used as a wetting liquid.

To determine the contact angle of the electrospun fibers, they were made more compact for accurate measurement. First, the WCENFs on the PP substrate was placed upside-down on the PET sheet and subjected to thermal press for 10 seconds at a temperature of 120 °C, and then, PP was detached. Next, the WCENFs on PET were covered with a glossy sheet for a thermal press again with the same conditions to acquire a smooth and more compact surface. This step was done so that liquid could stay on the surface for angle measurement; otherwise, the surface would not hold the drop in the case of WCENFs alone or with PP substrate, and it would instantly settle down and penetrate through the structure. Finally, the contact angle of electrospun fibers was measured using the sessile drop technique on a goniometer (Surface Energy Evaluation System (SEE System), Advex Instruments, Brno, Czech Republic) at ambient temperature. A 5 µl pipette was used to drop liquid on the sample surface (10×10 mm^2), the drop shape was observed using a CCD camera, and the angle was measured instantly. Glycerol and Milli Q water were used as the probe liquids to determine hydrophilicity. The samples were analyzed in triplicates, and the mean values with standard deviation were reported.

The thermal stability of the fibers was determined using a TGA Q500 thermogravimetric analyzer (TA Instruments, USA). Sample mass (~19.0±0.5 mg),

Table 1. Representative properties of the solution prior to electrospinning and of produced WCENFs compared with CA fibers [50].

Sample	Concentration [%]	Density [g/cm^3]	Intrinsic viscosity [Pa·s]	Electrical conductivity [µS/cm]	Average area mass [g/m^2]
WCENFs	8	1.320	0.95	88.1	0.865
CA	9	1.315	1.64	83.4	1.630

depending on its density, was heated in alumina crucible from 25 to 700 °C at a ramp of 15 °C/min under N_2 flow of 100 ml/min. To determine the thermal behavior and properties of WCENFs, they were subjected to differential scanning calorimeter (DSC) star®System (Mettler Toledo, Switzerland). The sample mass (5.0±0.5 mg) was sealed in an aluminum pan under a nitrogen flow of 50 ml/min and heated from 25 to 320 °C at a ramp of 10 °C/min.

Gel permeation chromatography (GPC) used a Waters HPLC system equipped with a Waters model e2695 and a Waters model 2414 differential refractometer to determine the average molar mass (M_w), number average molar mass (M_n), and polydispersity index ($PDI = M_w/M_n$) of the tested WCENFs samples from peaks corresponding to the polymer fraction using the absolute calibration method (Waters Corporation, Milford, USA). The WCENFs was dissolved in THF (2–3 mg/ml), stabilized with BHT (240 mg/l), and filtered through a 0.45 µm syringe filter. The following procedure was used to separate the samples on a series of gel-mixed bed columns (Polymer Laboratories Ltd, Shropshire, UK): 1 × PLgel-Mixed-A bed column (300×7.5 mm, 20 µm), 1 × PLgel-Mixed-B bed column (300×7.5 mm, 10 µm), and 1 × PLgel-Mixed-D bed column (300×7.5 mm, 5 µm); at 40 °C, the mobile phase contained THF stabilized with BHT (240 mg/l). The mobile phase flow rate was set to 1.0 ml/min, and the injection volume was 100 µl. All data processing was carried out using Empower 3 software.

To see the strength of fibers, the tensile test of neat PP and PP substrate with WCENFs was performed and compared because pure WCENFs were very fragile, it was difficult to peel them from the PP sheet to prepare a dumbbell shape and perform a tensile test. Further to test the WCENFs as syringe film in the last section, PET was used as a support substrate for WCENFs. Therefore, the tensile tests of PP, PP/WCENFs), and PET/WCENFs were carried out on an M350-5CT tensile testing machine (Testometric, UK) supplied with a load cell of 10 kgf. For all measurements, a crosshead pull speed of 10 mm/min and a gauge length of 20 mm was used. A unique die was used to cut specimens in the shape of dumbbells (Type 3, ISO 37:2005). Young's elastic modulus [MPa], ultimate tensile strength [N/mm], percentage elongation [%], and other mechanical properties were obtained. Measurements were conducted in triplicates, and mean values with standard deviation were reported.

2.4. High-performance liquid chromatography (HPLC) analytical method

A HPLC DionexUltiMate 3000 Series (Thermo Fisher Scientific, Germany) was used to analyze EH (E1, E2, EE2, E3) calibration standards and samples. The separation was carried out at 30 °C on a Kinetex 2.6 µm C18 100 A (150×4.6 mm; Phenomenex, USA) reversed-phase column with a pre-column security guard ULTRA, UHPLC C18 (Phenomenex, USA). A mobile phase of acetonitrile and water (45:55, vol/vol) was utilized at a flow rate of 0.8 ml/min for a total isocratic run of 12 min. A volume of 20 µl was injected into the column, and the sampler chamber was set at 5 °C. The eluates were recorded, and the EH concentrations were determined using the 200 nm test results. The external calibration method for EH concentration quantification was performed using the Chromeleon version 7.2 software (Thermo Fisher Scientific, USA) [52].

2.5. Solution preparation and sampling

Preliminary experiments were carried out to determine the exact concentration when all four EH were completely dissolved together in a mixture. The solubility of individual hormones was lower than the values available in the literature. When 1 mg/l concentration of each EH was prepared separately, it was observed that E1 partially remained undissolved after 24 h of stirring, with some solute particles staying at the bottom of the container. A similar observation was reported by Han *et al*. [13] that it took 12 days for E1 to reach a plateau concentration of 0.61 mg/l. Therefore, considering a solution with a mixture of four different EH, it was necessary to have a lower solution concentration from this value. The method of EH detection and quantification via HPLC was developed earlier. Hence, a solution containing all four EH was prepared by adding 1 mg of each EH in a total of 5 l of water, kept under magnetic stirring at 800 rpm for 24 h, making an overall concentration of 0.8 mg/l solution with the individual concentrations of 0.2 mg/l. For calibration, samples in a concentration of 0.2, 0.15, 0.1, 0.05, 0.03, 0.02, 0.005 mg/l were collected using a micropipette (HTL Lab Solution, Poland) in 1.5 ml screw neck vials (VWR, Czech Republic) after passing through glass microfiber (GMF) filter (Whatman, Czech Republic) with pore size 0.45 µm and 25 mm in diameter before placing in HPLC. A calibration curve was

obtained using mean concentrations from the triplicate values. The calibration vial with a concentration of 0.005 mg/l was used to identify each hormone's detection limit. The limit was set at 0.5, 1.0, 2.0, and 5.0 µg/l for E3, E2, EE2, and E1, respectively [52].

2.6. Batch adsorption test of WCENFs

The experimental kinetics were carried out to determine the adsorption rate. Tests for WCENFs were performed in triplicates using 100 ml of EH solution taken from stock with a total concentration of 0.8 mg/l, and 20 mg of WCENFs were placed in each flask. The flasks were continuously stirred at 250 rpm using an orbital incubator shaker (GFL 3005, MERCI s.r.o., Germany). To determine the remaining concentration of EH present in the solution, samples were drawn at fixed intervals of time each after 5, 15, 30, 60 min, and after each hour until a plateau was reached. At each specified time interval, 4 ml samples were drawn carefully without any contact with fibers using a 20 ml syringe and collected in vials after passing through a 0.45 µm GMF filter. The first 2 ml filtrate was discarded by passing from a syringe through a GMF filter to eliminate any negligible adsorption within the filter and rinse out any remaining liquid from the previous reading while sampling to ensure accuracy and precision. Proper care was taken to ensure that neither fiber was removed nor destroyed during the sampling and was replaced by 4 ml of ultrapure water to maintain the total flask volume. A control flask containing only solution was also placed as a starting reference concentration in the experiment. It must be noted that negligible adsorption was observed on the glass surface of the flask throughout the experimentation, which was calculated by comparing the initial measured concentration with the concentration of control after 9 h of shaking. Then, the results of triplicated experimental values were obtained to calculate mean concentration values and standard deviations that were recorded and reported. Finally, the percentage of adsorption of each EH on WCENFs was calculated with reference to the control. The solution was maintained neutral at a pH of 7.3 using ultrapure deionized water because river water samples are in the pH range of 6–9. The percentage removal of each EH at a given time (t) was measured using the expression shown in Equation (1) [53]:

$$Removal\,[\%] = \frac{C_i - C_t}{C_i} \cdot 100 \tag{1}$$

where C_i is the initial concentration [mg/l] and C_t is the concentration of solution at time t [mg/L].
Also, equilibrium adsorption capacity (q_e) and adsorption capacity (q_t) at time t can be calculated by the following expressions shown in Equation (2) and (3):

$$q_e = v \cdot \frac{C_i - C_e}{m} \tag{2}$$

$$q_t = v \cdot \frac{C_i - C_t}{m} \tag{3}$$

where m is the mass of adsorbent in grams, C_e is the concentration of the solution at equilibrium. and v is the volume of solution in liters.

2.7. Desorption and reusability of material

To determine the reversibility of WCENFs sorption, the fibers in triplicates were taken out from the EH solution and washed thoroughly with distilled and deionized water followed by immersion in 50 ml of water and shaken for 20 min at 250 rpm. This step would just clean the surface of fibers and nominally remove some physically adsorbed hormones, but it would not significantly reduce EH concentration on fibers due to chemical bonding [9]. The fibers were then placed in the oven at 30 °C for 6 h to remove the excess moisture, followed by air drying without any effect on fibers. This step was performed in triplicates by immersing the fibers in 40 ml pure anhydrous ethanol, given that all estrogenic hormones have a very high solubility in ethanol based on their high partitioning coefficient (log K_{ow} = 3.13, 4.01, 2.45, and 3.90 for E1, E2, E3, and EE2, respectively). Then, a strong partition effect was expected to occur in combination with a competing hydroxyl group present in ethanol that could destabilize the EH-fiber hydrogen bonds and attract the adsorbed hydrophobic hormones in the ethanol solution [13, 54]. Next, the solution system was gently stirred for 30 min at 175 rpm for complete elution of EH from the fibers; after that, air-dried at room temperature and placed in a desiccator until used for the next adsorption cycle. The procedure was repeated for several cycles until very low adsorption was expected.

2.8. Instantaneous adsorption test of PET/WCENFs syringe film

To perform the syringe film test, the WCENFs, due to their fragility, were preferably compressed on the PET sheet and used instead of WCENFs alone or with PP sheet because PP can itself adsorb hormones as previously reported at 96.3% of E1 using a 0.2 µm membrane film [13]. In addition, PET is stiffer to hold fiber straight as a film, providing better strength and enduring high pressures during the filtration process [55]. Therefore, the adsorption of EH was first tested on a neat PET mat to see any influence of adsorption. A batch adsorption test was conducted in the same manner as for WCENFs previously, and no adsorption of any EH was observed on PET. The HPLC chromatograms of solution before and after adsorption perfectly overlap, and no decrease was observed in EH concentration (Figure 1). Then, WCENFs compressed on a PET sheet were cut into a 25 mm circular disc in triplicates and placed in the Swinnex film holders.

3. Results and discussion

3.1. Characterization of adsorbent

SEM imaging was carried out for morphological analysis of the electrospun fibers.

Figure 2 illustrates that uniform submicron fibers were produced with minimum possible beads and a relatively narrow fiber diameter distribution of 196±65 nm compared with the CA having 224±35 nm and calculated surface area of 13.6 m^2/g [50]. This indicates that WCENFs possess a higher surface area of 15.5 m^2/g (Table 2) and more available adsorption sites. Such low average diameter is attributed to properties mentioned in Table 1: lower intrinsic viscosity, low polymer concentration in the solution, and high electrical conductivity prior to electrospinning, which has led to the development of a high surface area of WCENFs. Also, the molecular properties calculated from GPC were M_n = 90 000 g/mol, M_w = 210 000 g/mol, and PDI = 2.3. To further understand the physicochemical properties of the structure, XRD results revealed a broad single peak near 2θ = 15°, which denotes that WCENFs are semi-amorphous by nature [56]. The functional groups are further discussed in FTIR. The mean diameter of pores in the submicron structure was 1.4 µm, and the maximum pore diameter was 2.2 µm. The permeability of the submicron structure for the dry air was 247 l/(min·bar·cm^2). Also, the results from the TGA thermograph showed no material degradation was observed up to 110 °C, and the degradation temperature was found to be 355.7 °C [45]. The initial dip in DSC thermogram could be due to evaporation of water and the graph revealed that the glass transition temperature (T_g) of WCENFs was well above standard room operating temperatures (~180 °C) and given that the material's degradation range started around 250 °C and was spread over a wide range. The thermogram indicates that the material was thermally stable; therefore, these fibers would not be subjected to any softening and deformation at room temperature during the whole adsorption studies [5, 8]. ImageJ analysis software obtained the average diameter of fibers observed through SEM. Considering the fiber as a single continuous cylinder, the length per unit mass [l/m] and surface area (A) of the fiber can be calculated using the expressions given in Equation (4), and (5) [9]:

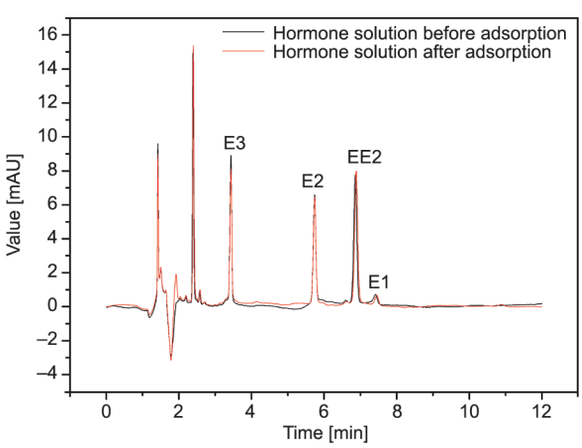

Figure 1. Chromatogram of before and after adsorption on PET with stock solution (0.8 mg/l) containing 0.2 mg/l concentration of each EH (E3, E2, EE2, E1) in a mixture.

$$V = \frac{m}{\rho} = \frac{\pi d^2 l}{4} \tag{4}$$

By rearranging this expression, we get:

$$\frac{l}{m} = \frac{4}{\rho \pi d^2} \tag{5}$$

where V is the volume [m^3], m is the mass [mg], d is the diameter of fiber [m], and ρ is the density of material [1.32 g/cm^3].

Since $l \gg d$; therefore, individual cross-sectional area (A) of the end corners of the fibers can be neglected, and the total surface area per unit mass can be expressed as (Equation (6)):

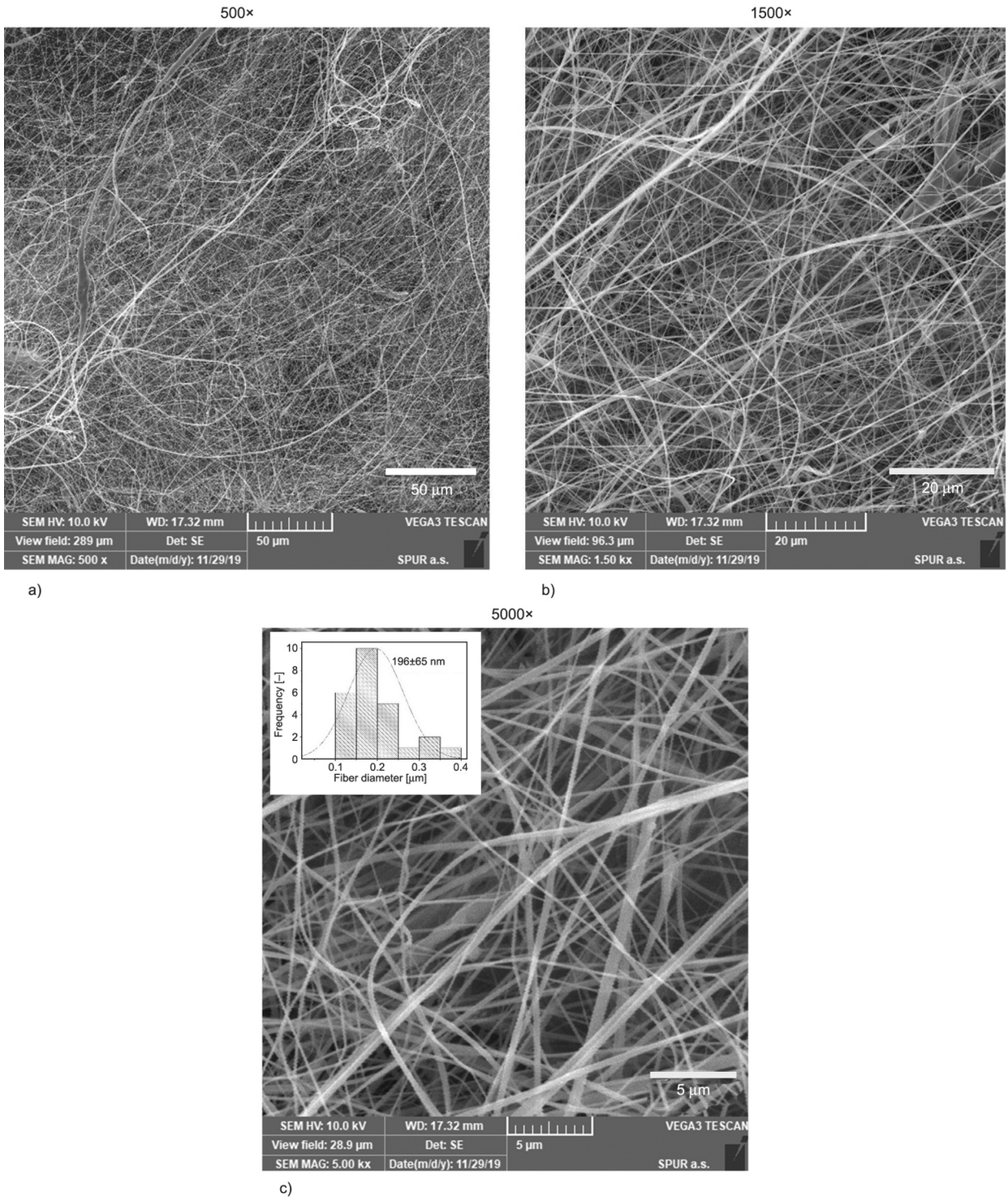

Figure 2. SEM micrograph and (inset) size distribution for WCENFs at different magnification of (a) 500×, (b) 1500× and (c) 5000×.

$$\frac{A}{m} = \frac{d\pi l}{m} = \frac{4}{\rho d} \tag{6}$$

The calculated diameters from the SEM images, calculated fiber length, surface area using the above formulas, the surface area measured by BET, and porosity by porometry are shown in Table 2.

The geometrically determined surface area based on SEM compared to that by BET analysis is well in compliance. The BET surface area is well comparable to the literature values in the range of 9–51 m^2/g and the average fiber diameter of 167–2737 nm [9]. The calculated surface area from the average fiber diameter (196±65 nm) considered as cylindrical

Table 2. Characteristics values of WCENFs calculated using SEM micrographs, BET, and porometry.

BET before adsorption		BET after adsorption		Porometry		Fiber analysis from SEM	
Surface area [m^2/g]	18.05	Surface area [m^2/g]	3.61	Mean pore size porometry [µm]	1.4	Average fiber diameter [nm]	196±65
Mean pore diameter [nm]	13.49	Mean pore diameter [nm]	17.19	Maximum pore size porometry [µm]	2.2	Fiber length per unit mass calculated [m/mg]	25 105
Total pore volume [cm^3/g]	0.061	Total pore volume [cm^3/g]	0.016	Air permeability porometry [$l/(cm^2 \cdot min \cdot bar)$]	247	Calculated surface area [m^2/g]	15.5

shape calculated from SEM is 15.5 m^2/g. The actual surface area measured from BET is 18.05 m^2/g which is slightly higher. The plausible reason for lower calculated surface area value based on geometry compared with BET value could be due to much lower density than the bulk polymer density because of pore formation and other effects during electrospinning. The presence of pores on the fibers' surface is confirmed by BET mean pore diameter (13.49 nm). Furthermore, the estimated surface area is based on the assumption that the fibers have a smooth surface without pores. In reality, solvent evaporation during electrospinning has resulted in a smaller diameter of fibers seen from the SEM micrograph (Figure 2), which has resulted in increased surface area. We can also see that the surface area of fiber decreased after four adsorption cycles from 18.05 to 3.61 m^2/g due to interaction with ethanol during desorption cycles that caused swelling (discussed in detail in the reusability section). However, the mean pore diameter increased from 13.49 to 17.19 nm due to the wear-off of material during several desorption cycles. Still, a reduced total pore volume was observed from 0.061 to 0.016 cm^3/g, which justifies the adsorption and entrapment of hormones in the fibers during interaction in the batch adsorption study.

The contact angle was measured to determine the hydrophilicity of the fibers. WCENFs mainly contain CA, which has polar hydroxyl groups. Thus, CA is hydrophilic by nature [57]. We observed both the liquids penetrated the WCENFs on PP completely. Therefore, WCENFs were compressed on a PET sheet, and they exhibited contact angle values of 14.6±3.3° with water and 87.3±0.8° with glycerol. It is generally agreed that a hydrophilic surface shows a low water contact angle ($\theta < 90°$). It is reported that the surface roughness, average fiber diameter, and concentration of the polymer in the solution before electrospinning also have a direct influence on the wetting properties [57, 58]. The reported electrospun CA in the literature had a water contact angle of 22.2±0.9°, which is higher compared to the water contact angle of WCENFs (14.6±3.3°) in the current study; This indicates that WCENFs are slightly more hydrophilic compared to electrospun CA in literature [50]. The investigated WCENFs in the present research possess a low contact angle which indicates high hydrophilicity. The hydrophilic nature of WCENFs provides feasibility to the fibers to interact with EH in water and support the adsorption process because the stronger interaction between EH and WCENFs is due to the hydrogen bonding interaction and Van der Waals forces which essentially requires the hydrophilic nature of the fiber [59].

To see the mechanical properties of WCENFs, the stress vs. strain graph below explains Young's modulus, ultimate tensile strength, maximum elongation before fracture, and stress at breakage.

Figure 3 demonstrates the stress *vs*. strain curve of PP and PP with WCENFs up to the breaking point. It can be seen that Young's modulus has increased from 8.9 to 28.8 MPa, which is evident from the steep slope in the graph, and the ultimate tensile strength has improved to almost 122% (3.1 to 6.9 N/mm^2). Similarly, a slight increase in stress at breakage from 0.4 to 1.4 MPa and the total elongation from 19.3 to 19.9 mm was observed, showing that the difference between the two values in each case determined the value of that physical quantity of WCENFs. Similar values of the mechanical properties of electrospun fibers were reported in the literature [51].

However, throughout the batch adsorption study, WCENFs were used alone after peeling off from the PP sheet, which was only used for the collection of fiber. Herein, PP was used as a support material for measuring mechanical properties as alone WCENFs were too fragile and could not maintain shape after peeling off owing to their weak inter-fiber adhesion [51], low average area mass (0.865 g/m^2), and thickness (0.003 mm) compared to CA spun fibers with 1.630 g/m^2 and 0.005 mm, respectively. The mean values for each sample are reported below in Table 3.

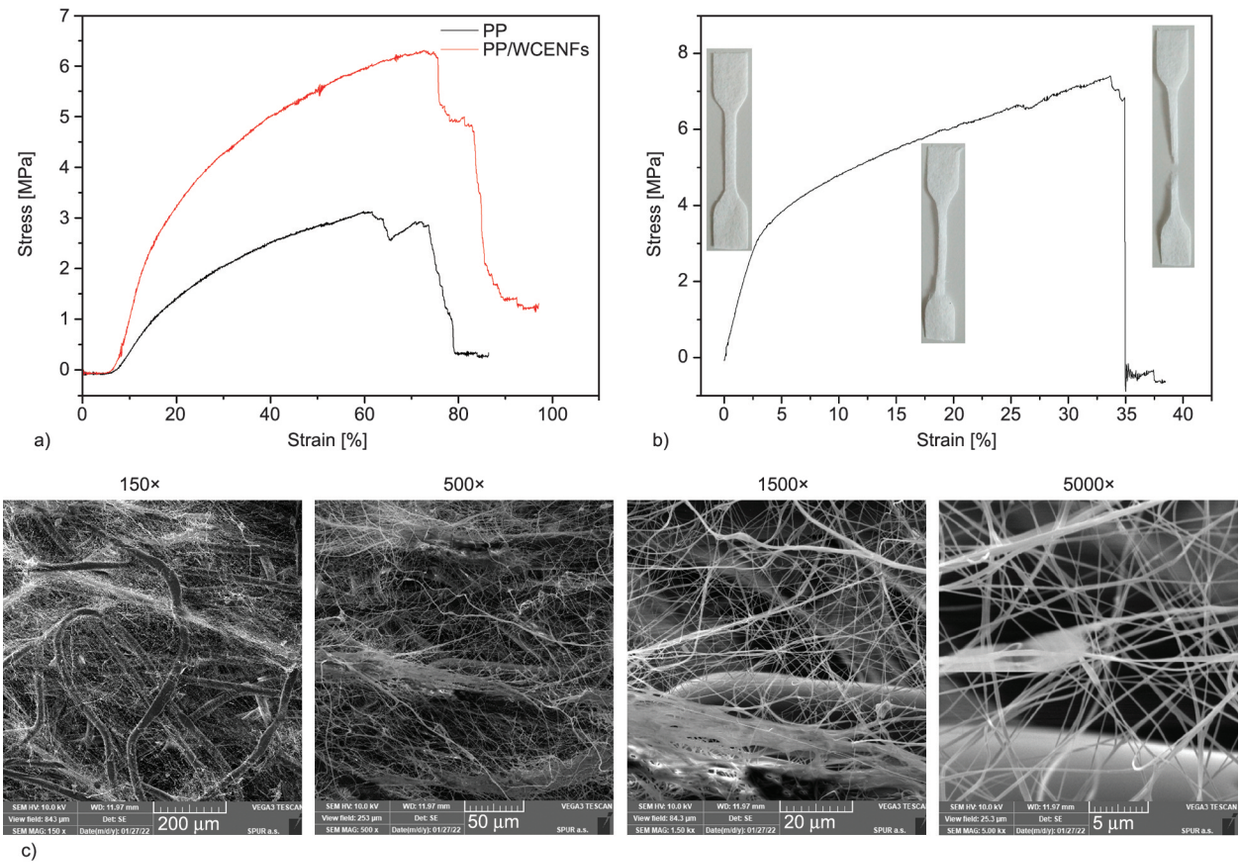

Figure 3. Stress vs. strain curves for (a) PP and PP/WCENFs, and (b) PET/WCENFs along with micrographs after breakage at a different magnification of 150×, 500×, 1500×, and 5000×(c).

Table 3. Summary of mechanical properties of the WCENFs with substrates.

Materials	Thickness [mm]	Young's modulus, *E* [MPa]	Ultimate tensile strength, σ [N/mm^2]	Elongation at break, ε [mm]	Stress at break [MPa]
PP	0.14±0.01	8.9±4.3	3.1±1.0	19.3±5.1	0.4±0.2
PP/WCENFs	0.17±0.01	28.8±2.4	6.9±1.2	19.9±0.7	1.4±0.2
PET/WCENFs	0.14±0.01	109.0±23.1	7.5±0.9	8.6±1.3	0.1±0.4

Similarly, the mechanical properties were observed for the fabricated PET/WCENFs syringe film, and an improvement in strength and Young's modulus was reported to be 7.5 N/mm^2 and 109 MPa, respectively. PET/WCENFs film was used for the syringe adsorption test to compare the removal percentage with the commercial CA syringe film. Herein, WCENFs were embedded on a PET sheet of thickness 0.43 mm by the thermal press. The significant increase in each mechanical property is illustrated in Table 3, and micrograph images at different magnifications are represented in Figure 3 to see the behavior at the time of fracture. It can be seen that the strength for elongation is primarily provided by the PET sheet, which breaks following the ductile failure, whereas WCENFs were relatively brittle. They gradually broke after a slight elongation when the fiber chain straightened up (evident at 500× and 1500× magnification) owing to their non-woven and non-crosslinked structure [44]. It can be seen that only a few fiber treads remained intact over a long elongation. The results also reveal that the PET/WCENFs film can be used for continuous filtration removal of hormones in future research.

3.2. Batch adsorption study of EH on WCENFs

The study of four EH (E1, E2, EE2, E3) was conducted with a total concentration of 0.8 mg/l and 20 mg of WCENFs. Figure 4a below shows the batch adsorption study of each hormone on WCENFs for a period of time till no further significant adsorption was observed and the material reached almost saturation.

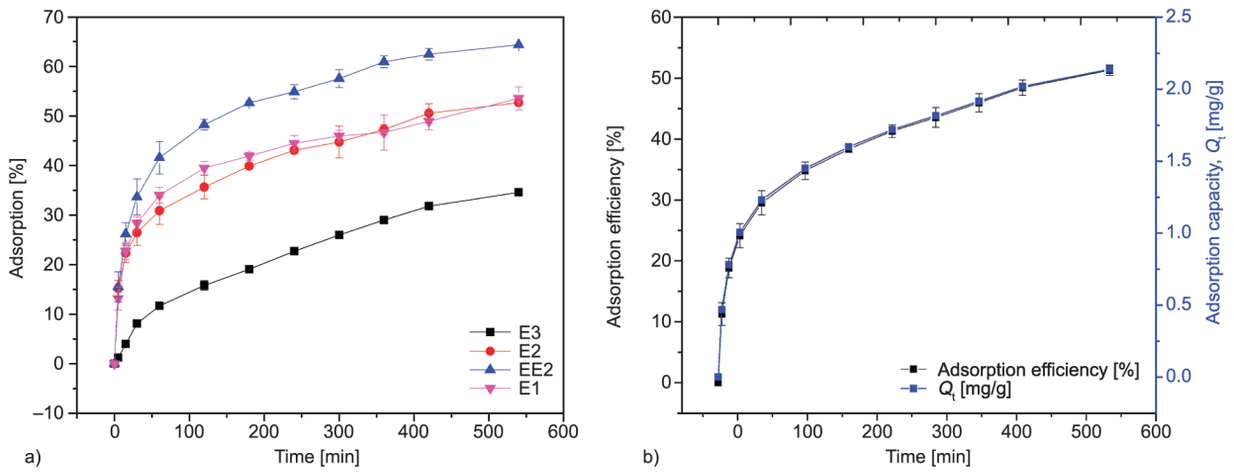

Figure 4. (a) Batch adsorption study of each EH on WCENFs from a combined solution, (b) cumulative adsorption removal efficiency as a function of time of EH (E1, E2, EE2, E3) together on WCENFs on the primary y-axis, and the total adsorption capacity (Q_t) of WCENFs as a function of time on the secondary *y*-axis.

Figure 4a depicts WCENFs adsorption behavior with each hormone, and as can be seen, the ascending order of adsorption of EH is as E3 < E2 < E1 < EE2 with removal efficiencies of 34.6, 52.7, 53.6, and 64.3%, respectively. WCENFs showed the best sorption of EE2 and the worst sorption of E3 hormone. It could also be concluded that WCENFs can readily adsorb EE2, E2, and E1, while gradually adsorb E3. The low percentage removal of E3 could be attributed to its low log K_{ow} value; 2.45, compared to E1, E2, and EE2; 3.43, 3.94, and 4.15, respectively. Log K_{ow} is a parameter used to determine the value of hydrophobicity for EH by measuring the partitioning between water and octanol. The values are ranged between –3 (very hydrophilic) and +10 (extremely hydrophobic). Generally, the values above 2.5 indicate that the material would accumulate in the solid phase and not be dissolved in an aqueous medium. Therefore, its interaction with the membrane would be hydrophobic. High log K_{ow} values tend to adsorb more readily to organic matter because of their low affinity for water [59]. The adsorption of these estrogens is directly dependent on their hydrophobic nature, which is specified by the higher value of K_{ow} [60]. Furthermore, E3 follows a different kinetic trend than the other EH because the adsorption is gradual throughout the experiment. While for other EH, most of the adsorption occurs within 30 min from the starting time. WCENFs have similar adsorption behavior for all EH compared to the CA fibers, which also follows adsorption efficiency in decreasing order of EE2 > E1 > E2 > E3. However, the removal efficiencies of EH with WCENFs are more significant than CA electrospun fibers [50]. Hence, it can be concluded that electrospun WCENFs can be sufficiently responsible for the adsorption of each EH simultaneously.

Figure 4b above shows the percentage of total cumulative adsorption of EH on WCENFs and the total adsorption capacity of WCENFs in a given time. The results show that the total equilibrium removal efficiency lies at 51.3%. It is evident from the graph that WCENFs had a high adsorption tendency and fast adsorption rates reaching nearly half of their efficiency within the first 30 min, as represented by the steep initial slope of the graph corresponding to the removal efficiency mark of about 25%. However, the trend of gradient changed from steep to steady after almost 60 min of the continuous adsorption experiment and remained the same till the end.

The total adsorption capacity (Q_t) as a function of time is also demonstrated in Figure 4b with a secondary *y*-axis. The results indicate that the cumulative of four EH adsorption capacities increased similarly for WCENFs until equilibrium was established between the adsorbates and adsorbent. The time to reach equilibrium depends on the concentration of adsorbate and the amount of adsorbent. Both factors were kept constant to compare the capacities with the literature. However, it was still necessary to increase the amount of adsorbent to enhance the removal efficiency with a lesser time. The equilibrium adsorption capacity of WCENFs was found to be 2.14 mg/g, and adsorption capacities of E1, E2, EE2, and E3 were found to be 0.551, 0.532, 0.687, and 0.369 mg/g, respectively. Compared to the literature,

Yasir *et al*. [50] in previous research reported the equilibrium adsorption capacity of CA to be 2.095 mg/g and individual adsorption capacities of E1, E2, EE2, and E3 to be 0.506, 0.532, 0.668, and 0.389 mg/g, respectively. Therefore, the results of WCENFs are well in the range and strongly comply with the literature values of CA, which indicates that WCENFs are better in adsorption than electrospun CA fibers. Additionally, the as-prepared WCENFs are a cost-effective and efficient substitute.

Additionally, in the previous work, the highest equilibrium adsorption capacity was observed for PU Elastollan of 2.51 mg/g and the lowest for PAN of 1.51 mg/g. Furthermore, the reported adsorption capacities for E1, E2, EE2, and E3 were 0.801, 0.592, 0.736, and 0.382 mg/g for PU Elastollan and 0.396, 0.370, 0.343, and 0.397 mg/g for PAN, respectively [50].

Moreover, EE2 was found to have a strong affinity for adsorption as a result; highest adsorption capacity compared to the other three EH for all the other polymers mentioned in the literature. The adsorption capacities for MWCNTs in literature were found to be 0.423, 0.472, and 0.472 mg/g, and for the activated sludge were 2533.34, 2020.78, and 2234.09 ng/g for E1, E2, and EE2, respectively, which are lower values compared to the current research. Furthermore, the value for removing E1 was 62 ng/g when a hydrophobic hollow fiber membrane was used [60]. Thus, comparing the present study's adsorption capacity with the previous research works proves the suitability of WCENFs as a potential adsorbent for removing these EH comparing the other solid particles and membrane adsorbents. Hence, it is evident that WCENFs have a pretty high adsorption capacity and is a useful polymeric material for reusing it for these EH adsorption.

3.3. Adsorption kinetics

The removal of EH on WCENFs by adsorption increased with time, obtaining a maximum value for reaching equilibrium. The adsorption rate was fast initially until 30 min and gradually decreased as the contact time increased to an assuming plateau at 540 min. The results obtained from the experiment were used for studying the factors affecting the adsorption process and the rate-limiting step in this process, such as transfer of mass and type of chemical interaction processes. In addition, kinetics information helps select optimum conditions for full-scale removal of the EH process. However, it is often difficult to determine the kinetic parameters and explain the mechanisms involved in the complex heterogeneous systems because the surface effects can superimpose on the chemical effects. Therefore, to further understand the adsorption behaviors and mechanism, parameters from five models; Pseudo-first-order, Pseudo-second-order, and Weber-Morris intra-particle/membrane diffusion, Elovich and fractional power model equations were used to test the experimental data to examine the adsorption kinetics of four EH uptaken by WCENFs. These models are used best to describe the liquid/solid systems. The pseudo-first-order by Lagergren is a widely used and most common model for any adsorption study of different solutes in an aqueous solution. It explains that the rate of sorption of EH on the surface of the fibers is proportional to the number of hormones adsorbed from the solution phase, and it can be expressed by Equation (7) as [53]:

$$q_t = q_e\left(1 - \exp\left(-k_1 t\right)\right) \tag{7}$$

where q_t is the amount of hormone adsorbed per unit mass at time t [mg/g], q_e is the amount of hormone adsorbed per unit mass at equilibrium [mg/g], and k_1 is the first-order rate constant [l/min].

The pseudo-second-order equation is related to the solid phase adsorption capacity and can usually predict kinetics behavior over a long adsorption range. In this model, surface adsorption is the rate-determining step involving chemisorption because of physicochemical interactions between the solid and liquid phases [61]. Therefore, the linear form of Equation (8) can be expressed as:

$$\frac{t}{q_t} = \frac{1}{k_2 q_e^2} + \frac{t}{q_e} \tag{8}$$

where k_2 is the reaction rate constant [g/(mg·min)]. Usually, the adsorption process occurs in consecutive steps; these include movement of the adsorbate from the solution bulk to the surface of the adsorbent and then diffusion through the boundary layer to the outer surface of the adsorbent. It is followed by the adsorption on an available active site on the adsorbent's surface and, at last, intra-particle diffusion through pores. The Weber-Morris intra-particle/membrane diffusion model is diffusion-controlled; the adsorption rate directly depends on the speed at which an adsorbate can diffuse towards the provided

adsorbent. Therefore, this model is described using Equation (9) [62]:

$$q_t = kt^{\frac{1}{2}} + I \quad (9)$$

where k is the reaction rate constant [mg/(g·h$^{1/2}$)], and I is the y-intercept constant [mg/g], gives the information about the boundary layer thickness.

For the validity of this model, it is essential to note that the linear converging line for each EH must pass through the origin for intra-particle diffusion to be the rate-determining step.

In reactions where chemisorption is a dominant mechanism such that on the surface of the adsorbent, adsorbate is deposited without desorption of products, the rate of adsorption decreases with time as the reaction proceeds, and it is due to the surface coverage. In such reactions, the Elovich model is suitable for explaining the chemisorption process by expressing the following linear Equation (10) [60]:

$$q_t = \beta \ln(\alpha\beta) + \beta \ln t \quad (10)$$

where α and β are the coefficients such that α represent the initial adsorption rate [g/(mg·min)] and β represents the desorption coefficient [g/(g·min)]. These coefficients can be calculated from the slope and y-intercept of the plot given in Figure 5d.

The fractional power model is the more advanced form of the Freundlich equation, and the linear form is expressed in Equation (11) [63]:

$$\ln q_t = \ln a + b \ln t \quad (11)$$

where a and b are the coefficients in the expression and given that $b < 1$, the product of a and b is given as the specific adsorption rate at 1 min after the start of the experiment.

The adsorption kinetic plots for the adsorption of four EH on WCENFs are shown in Figure 5, and the obtained kinetic parameters from the models mentioned above are presented in Table 4.

The results were examined to obtain adsorption kinetics fits of adsorbate mixture of E1, E2, EE2, and E3 EH on the adsorbent fibers using several model plots. In Figure 5a, the plotting ln ($q_e - q_t$) *vs*. t for E3 hormone shows good compliance with the pseudo-first-order equation. The data points are shown together with the generated lines of best fits. The agreement between the data set is reflected by the high regression coefficient (0.962) for E3, and the equilibrium adsorption capacity calculated for E3 (0.368) is extremely close to the experimental value (0.369), which indicates that predicted adsorption capacity by this model is almost the same as the actual value. The rate constant k_1 is similar and in the range for all EH. However, this model appears less accurate for E2, EE2, and E1 for describing the initial stage ($t \leq 30$ min). The theoretical expected yield of 0.350, 0.444, and 0.306 seems unsatisfactory and far less than the actual 0.532, 0.687, and 0.551 for E2, EE2, and E1.

The lines plotted in Figure 5b of t/q_t *vs*. t must be linear to estimate qe and k_2 from the slope and y-intercept, respectively. The results indicated that the interaction of E2, EE2, and E1 with the material followed a line of best fit, completely matching the data set points. The regression coefficients are 0.99, and the calculated adsorption capacities of E2, EE2, and E1 are 0.544, 0.711, and 0.549 compared to the experimental values 0.532, 0.687, and 0.551, respectively. The slight difference indicates that the active sites were not homogenous on the surface because the adsorption rate is determined by the hormone concentration and the number of active sites available on the material [64]. These findings confirm the suitability of this model for describing E1, E2, and EE2 adsorption on WCENFs. Similar results were observed when comparing the results described in the literature for MWCNTs by Al-Khateeb *et al*. [60]. Whereas E3 shows an overall non-linear trend; instead, two linear portions can be seen. One for the first 60 min and the second for the time interval after 100 min. The plot in Figure 5b was used to determine the rate constant (k_2) and the calculated equilibrium adsorption capacity (q_e) expressed in Equation (8) to obtain the regression coefficient (R^2) shown below in Table 4.

Regarding Figure 5c of q_t *vs*. $t^{1/2}$, the graph for E3 is a linear plot with a comparatively high regression coefficient, but the plot does not pass through the origin. This specifies that the intraparticle diffusion is not entirely the rate-limiting step, which is likely to happen in the adsorption of the other three EH as well, as shown in Figure 5c. The plausible reason for EH could be that they do not converge properly and the overall best fits do not pass through the origin; this could be due to a surface effect that may have dominantly controlled the sorption process after an hour of time interval and be considered a diffusion-controlled

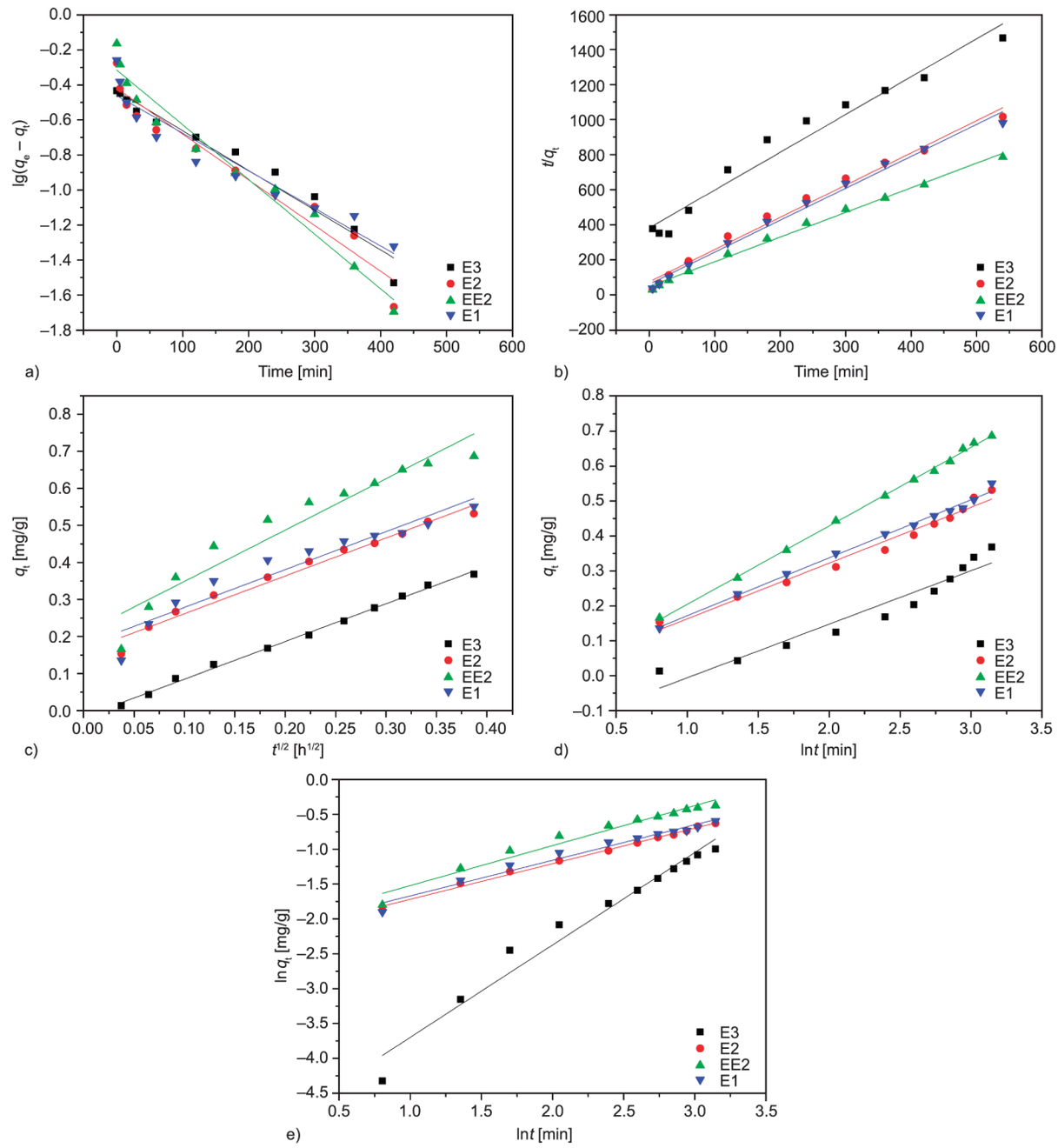

Figure 5. Adsorption kinetics plots of four EH (E1, E2, EE2, E3) on WCENFs, (a) Pseudo-first-order, (b) Pseudo-second-order, (c) Weber-Morris interparticle diffusion model, (d) Elovich model, and (e) fractional power model.

or boundary layer diffusion effect. Furthermore, two linear trends can be seen clearly. In the first 60 min, a sharper and steeper slope trend of a line is observed, which could pass through the origin and indicate that intraparticle diffusion is the rate-limiting step in this region. While in the second region, the diffusion slows down, shown by a gentle slope because the lesser remaining concentration of EH is left in the solution. Thus, for E2, EE2, and E1, intraparticle diffusion can be part of the mechanism, but it can not be a total rate-determining step [60].

The plot in Figure 5d of q_t *vs*. ln*t* shows that EE2 has the highest regression coefficient (0.999), which explains that chemisorption is the most prominent mechanism for the adsorption of EE2 on WCENFs. This is also proven when EE2 had the most rapid adsorption (see Figure 4a) and the highest equilibrium capacity of 0.687 mg/g compared to the other EH.

In the case of Figure 5e of lnq_t *vs*. ln*t*, a mismatch is seen for E3, while a linear relationship is seen for E1, E2, and EE2 but not for overall adsorption time. The regression coefficients are not satisfactory in

Table 4. The kinetic models parameters with each EH using WCENFs.

Models		Hormones			
Parameters		**Estrone (E1)**	**β-Estradiol (E2)**	**17α-ethinylestradiol (EE2)**	**Estriol (E3)**
Experimental q_e	[mg/g]	0.551	0.532	0.687	0.369
Pseudo first order model					
k_1	[min^{-1}]	0.002	0.003	0.003	0.002
$q_{e,cal}$	[mg/g]	0.306	0.350	0.444	0.368
R^2	[–]	0.951	0.958	0.977	0.962
Pseudo second order model					
k_2	[g/(mg·min)]	0.055	0.045	0.041	0.012
$q_{e,cal}$	[mg/g]	0.549	0.544	0.711	0.464
R^2	[–]	0.991	0.988	0.995	0.966
Intraparticle diffusion model					
k	[mg/(g·$h^{1/2}$)]	1.006	1.022	1.386	1.017
I	[mg/g]	0.181	0.159	0.210	–0.017
R^2	[–]	0.931	0.975	0.926	0.996
Elovich model					
α	[g/(mg·min)]	14.964	12.962	7.414	1.636
β	[mg/(mg·min)]	0.081	0.080	0.112	0.077
R^2	[–]	0.994	0.979	0.999	0.930
Fractional power model					
a	[–]	0.113	0.108	0.123	0.007
b	[–]	0.255	0.255	0.286	0.663
$a + b$	[–]	0.368	0.362	0.409	0.669
R^2	[–]	0.973	0.994	0.967	0.969

most of the cases. This indicates that the fractional power model is not appropriate for EH. The calculated parameters using Equations (7)–(11) are shown in Table 4.

3.4. Adsorption mechanism

The four possible adsorption mechanisms between EH and the WCENFs could be (1) size-exclusion; (2) physical adsorption of estrogens on the external surface and inside layers of fibers due to their porous structures; (3 charge interactions between EH and WCENFs; (4) Hydrogen bonding of EH molecules onto fibers by reaction with the functional groups present on the surface of fibers. Size exclusion is unexpected in this system because the reported molecular size of estrogens by Han *et al*. [54] is quite small (approximately 0.8 nm for E1 and 0.796 nm for E2) than the pore sizes of the WCENFs (1.4 μm) and GMF film (0.45 μm) used. Otherwise, the removal efficiency would have been 100%. A smaller fiber diameter in WCENFs (196±65 nm) leads to a larger surface area (15.5 m^2/g) that provides sufficient active sites for adsorption of EH on the fibers, as shown in Table 2. The electrostatic charge might also influence adsorption, as Porter and Porter already reported adsorption behavior on microfilms in the presence of cations [65]. The deprotonation of E1, E2, EE2, and E3 is governed by the hydroxyl group's dissociation attached to the benzene ring. The acid dissociation constants for E1, E2, EE2 and E3 are 10.34, 10.46, 10.4 and 10.38, respectively [59, 66]. They all have slightly weaker acidity than phenol (pK_a = 10). As a result of the high value of pK_a, most of the molecules for all these estrogens are undissociated; thus, they stay neutral in the solution mixture. As a result, it is unlikely that the influence of charge interaction can be the main factor for the significant adsorption of these EH on the fibers [13].

The high and rapid adsorption of the EH on the WCENFs is particularly interesting. The size of molecules is far tiny compared to the porosity of this structure. Therefore, the pore size has negligible dependence on adsorption. Apart from the physical adsorption, which gradually reaches equilibrium, the only rational explanation is the strong interaction of these EH with the fibers due to the hydrogen bonding. Hydrogen bonds are more robust than the van der Waals forces involved in the physical adsorption. Figure 6 below shows the chemical interactions of each EH with the WCENFs molecule.

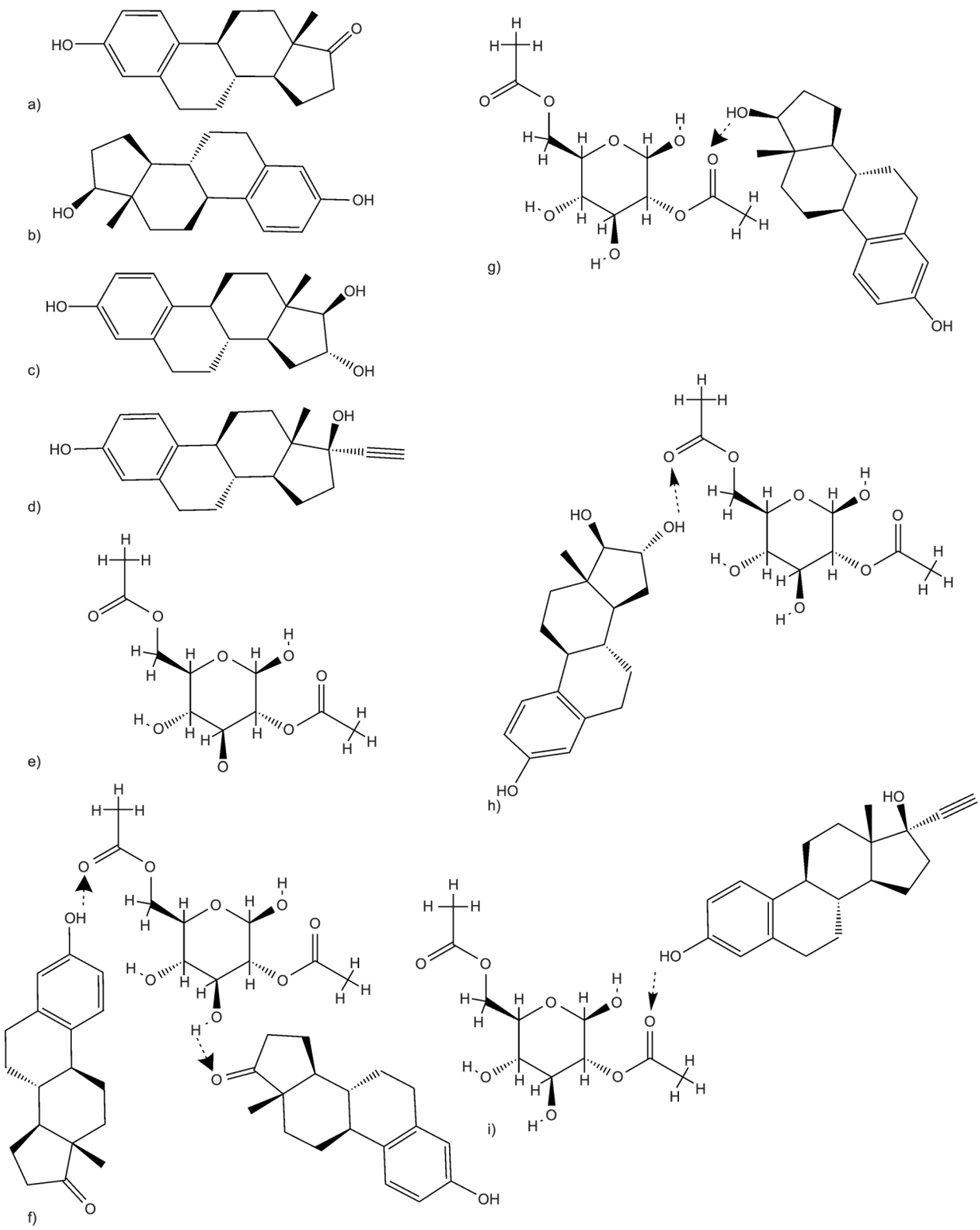

Figure 6. Displayed structures of (a) E1, (b) E2, (c) E3, (d) EE2, (e) WCENFs molecule and hydrogen bonding between WCENFs molecule with EH (f) E1, (g) E2, (h) E3, and (i) EE2.

The EH molecules (E1, E2, EE2, E3) in this study contain a hydroxyl group (–OH) acting as a proton donor for hydrogen bonding. Due to the presence of both nucleophilic carbonyl group (–C=O) and hydroxyl group in E1, this proton can act as both donor or acceptor in the hydrogen bonding because CA also contains both C=O and O–H groups. Han and coworkers [13, 54] have described and explained similar hydrogen bonding of E1 with nylon 6,6 membrane in their investigation. Nylon 6,6 and cellulose

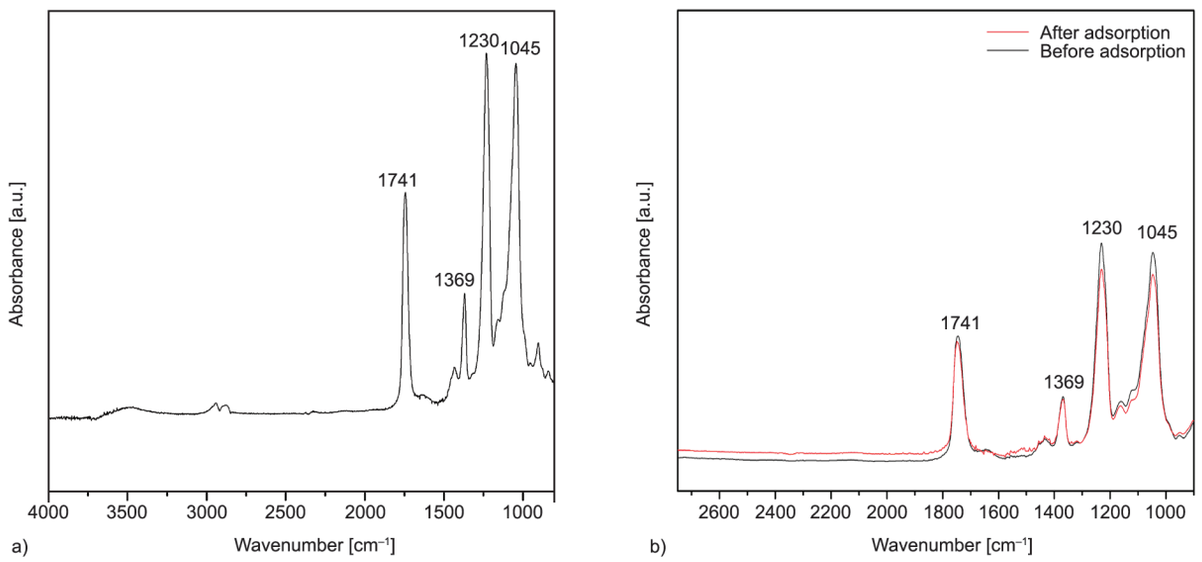

Figure 7. Attenuated total reflectance (ATR) mode FTIR spectra of (a) WCENFs and (b) before and after batch adsorption.

acetate have a common C=O functional group involved in the hydrogen bonding with the estrogens during the adsorption process. Therefore, the functional groups (C=O), (C–O–C), and (C–O–H) present in WCENFs are involved in hydrogen bonding due to lone pair electrons present on oxygen atoms with (C=O) and (O–H) groups present in E1, whereas only (O–H) group of the other three EH (E2, EE2, and E3) is involved in chemisorption as shown in Figure 6 and presented in FTIR analysis in Figure 7. These hydrogen bonding interactions would dictate the EH adsorption on WCENFs, explaining the fast adsorption process for EH in the initial stage of the experiment. FTIR analysis is a sensitive technique used in the study to characterize the hydrogen bonds on WCENFs, as shown below.

The ATR-FTIR characterization of WCENFs was performed to observe the functional groups present. The superimposed FTIR spectra of WCENFs before and after the adsorption study are presented in Figure 7. The broadband near 3400–3600 cm^{-1} indicates OH group presence in fibers. It is noteworthy to see a slight peak shift and the difference in the peak's relative intensities at 1741, 1230, and 1045 cm^{-1} corresponding to C=O stretching, C–O–C anti-symmetric stretching, and C–O bonds, respectively [67]. Their intensities significantly decreased after the adsorption study due to the developed inter-molecular hydrogen bonding interactions. In contrast, no change is noticed in the peak intensity at 1369 cm^{-1} belonging to the C–CH_3 bond because it can not undergo hydrogen bonding. This assures the existence of the chemisorption at 1741, 1230, and 1045 cm^{-1} of all these EH on the fibers' surface. In addition, the variation in the peak intensity depends on the number of active available functional groups present in the system and their competing behavior for the available sites [54]. Hence, the results supporting the previous literature suggest that EH (E1, E2, EE2, E3) could form hydrogen bonding with oxygen-containing groups on WCENFs. In our previous research, a similar study reported hydrogen bond interaction of carbonyl group (C=O) in polyurethane with these EH [50].

3.5. Determination of recovery and reusability

The adsorption and desorption process was repeated for four consecutive cycles, and considering the efficiency of WCENFs below 10% during the 4^{th} cycle, it was not further reused. The adsorption study of each cycle is reported in Figure 8.

Figure 8a represents the percentage removal of each EH concurrently on WCENFs during four consecutive adsorption cycles. As can be seen, the trend is decreasing after every successive cycle for all EH except for E3, where the adsorption percentage remains below 10% after the first cycle due to fewer available active sites for adsorption and intense competition among the functional groups of EH. The highest removal efficiencies are observed for EE2 (~64.3%), while least for E3 (~34.6%), and the trend is similar in each adsorption cycle. The gradual decrease in adsorption after each cycle is because of mass loss during the desorption process, leading to a reduction of

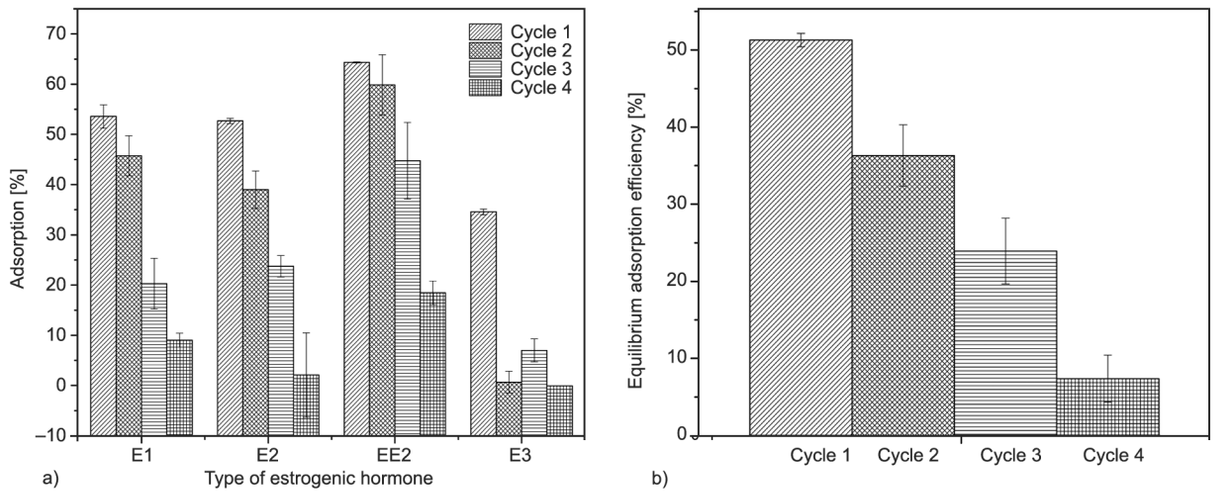

Figure 8. (a) Adsorption cycles of each EH (E1, E2, EE2, E3) with an initial concentration of 0.2 mg/l in a combined solution of 0.8 mg/l on WCENFs (20 mg), (b) cumulative efficiency of all EH adsorption on WCENFs during four cycles.

the active adsorptive sites and, thus, a drop in the surface area due to the increase in the fiber diameter (see Figure 9).

Figure 8b above illustrates the equilibrium adsorption efficiency of WCENFs for cumulative EH removal during four adsorption cycles. As can be seen, the highest reduction of EH in the first cycle is 51.3%, and the trend follows a gradual decrease which ends at 7.4% in the fourth adsorption cycle. Furthermore, it should also be noted that due to the continuous treatment with ethanol during desorption, it was evident that the fibers became stiff and shrank due to mass loss after the last cycle. Therefore, fibers were compact and tightly folded, providing less surface area for EH entrapment during the previous cycle. Thus, providing lesser removal efficiency. The presented comparison was made as a modeling study for the reusability of submicron structure from WCENFs for sorption. In industrial applications, some other solvents have to be tested. According to this model study, the more requested properties of a suitable solvent must be a very high solubility of EH with no solubility of the polymer.

With the repeated desorption cycles of EH from fibers using ethanol, there was a significant change in the fiber morphology attributed to the contact of fibers with ethanol. However, fibers were unlikely to dissolve in ethanol, and their porous structure allowed complete penetration of ethanol molecules. Therefore, after several cycles and contact time, it has led to collapse and swelling of the structure of the fibers and the effectiveness of the adsorption process [9]. It is evident in the SEM image of the fiber structure after the complete adsorption study, as shown.

Figure 9 shows the fiber's surface morphology after four adsorption-desorption cycles. As can be seen, the fiber's diameter increased from 196–351 nm, with the high swelling experienced on several fibers as shown above (white arrows).

3.6. EH adsorption on PET/WCENFs fabricated membrane film and commercial application

The adsorption equilibrium of EH solution was observed in these films, and a characteristic value of volume to reach equilibrium (V_{eq}) was noted. This concept of determining V_{eq} is used to conveniently and approximately mitigate the effect of these hormones simultaneously on WCENFs. V_{eq} is defined as the minimum volume of feed solution that passes through the film and can withstand to achieve adsorption equilibrium for this set of EH. Suppose the value of V_{eq} is significantly considerable; in that case, this method can instantly remove EH from wastewater. Figure 10 below shows the comparative results of E1, E2, EE2, and E3 adsorption on the PET/ WCENFs film, where the residual concentration of the mixed EH solution permeates normalized (expressed in percentage values) against the initial concentration of each hormone in the feed versus the accumulated feed solution. It must be noted that these results were compared with the commercial CA syringe film reported by Han *et al*. [13] for E1 adsorption.

Figure 10a shows simultaneous adsorption of all EH on the WCENFs film. It can be seen that the highest adsorption is experienced for E1 and the lowest for E3 until equilibrium was achieved at 7 ml of feed. It can be seen that maximum adsorption for E1, E2,

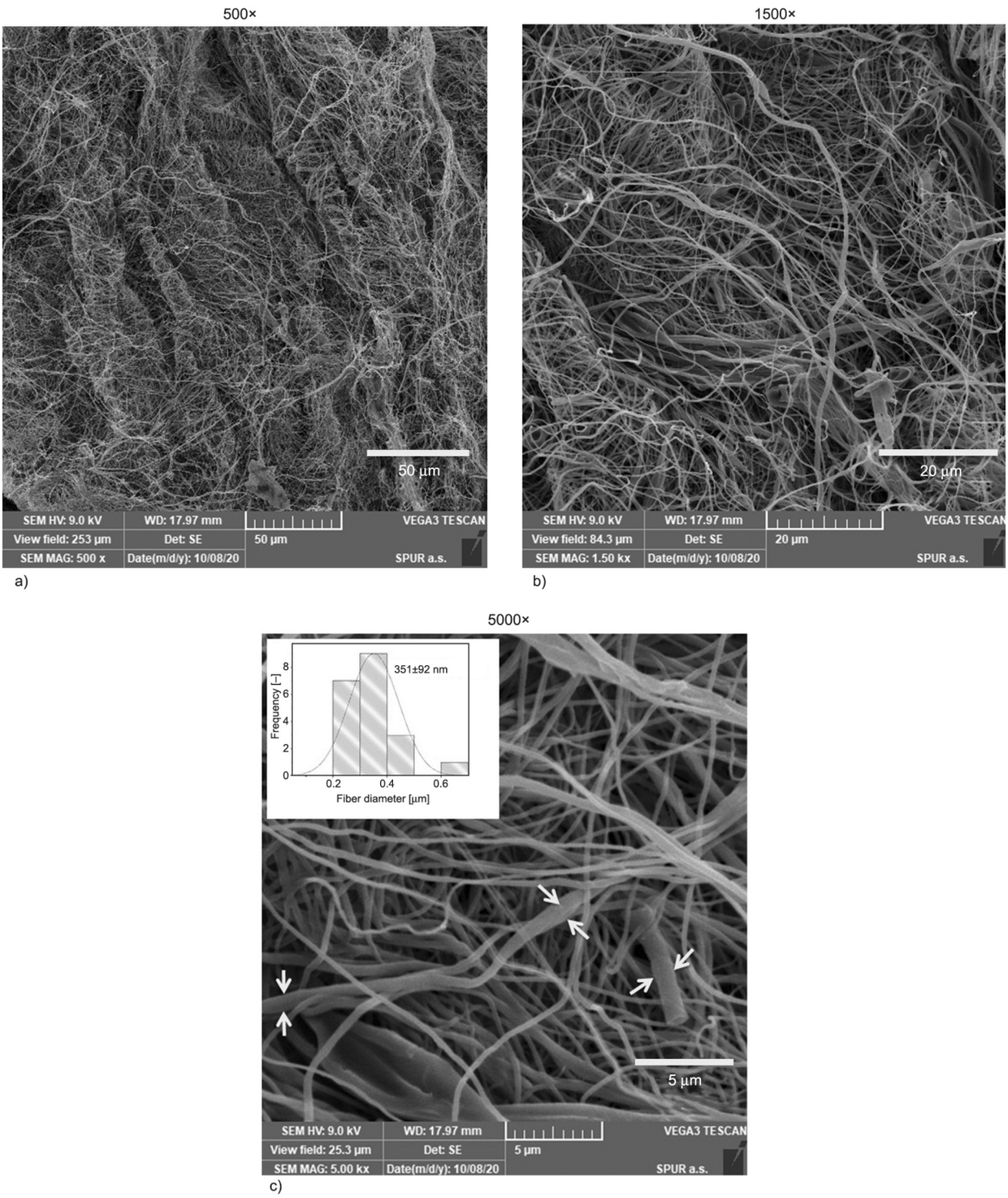

Figure 9. SEM image of WCENFs and their fiber diameter distribution after four adsorption-desorption cycles at a different magnification of (a) 500×, (b) 1500×, and (c) 5000×.

EE2, and E3 were found to be 24.5, 12.6, 19.7, and 0.5%, respectively. A gradual decrease in adsorption was seen for the PET/WCENFs film in a syringe adsorption test, which suggests the process of physical adsorption of EH on the PET/WCENFs film.

Figure 10b compares the results of WCENFs film with the commercial CA syringe film over 10 ml accumulated volume of feed. As can be seen, the total E1 adsorption of 18.6% was seen for commercial CA film with the initial solution concentration of 0.4 mg/l while 24.5% for WCENFs with the initial concentration of 0.2 mg/l. Also, 14.2% total adsorption on PET/WCENFs was noticed from the mixture of all four EH with the solution concentration

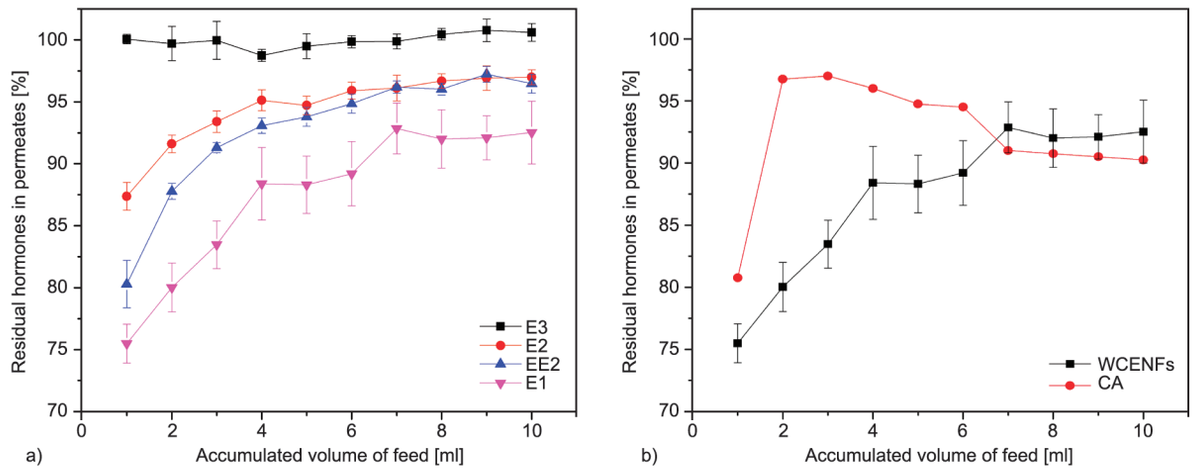

Figure 10. (a) Concurrent adsorption of EH (E1, E2, EE2, and E3) on 1.4 µm PET/WCENFs syringe film using 0.8 mg/l EH aqueous solution as feed containing 0.2 mg/l of each hormone and (b) 1.4 µm PET/WCENFs film adsorption comparison with 0.45 µm commercial CA syringe film for E1 [13].

of 0.8 mg/l, which is twice that of commercial CA. Furthermore, after the 1st mL of permeate passed through the commercial CA film, a decrease in adsorption was observed drastically during the next few permeates for commercial CA and then a slight increase in adsorption until it gets stagnant after 6 ml; this could be due to experimental error or loss of some already adsorbed E1 molecules on the surface of commercial CA film. While, a gradual decrease in adsorption was seen for PET/WCENFs syringe film, which suggests that physical adsorption could be the primary cause of EH adsorption but without any EH losses from the surface. The membrane's adsorption sites were occupied by EH molecules when more and more feed was passed, and eventually, an equilibrium was established when the adsorption sites were saturated. The derived V_{eq} value was 7 ml for both PET/WCENFs and commercial CA films. After these volumes, no significant change was observed. This suggests that the film reached saturation with EH at 7 ml. Similar results were reported in the literature for E1 adsorption reaching equilibrium at 8 ml for PP, 7 ml for polytetrafluoroethylene (PTFE), and 6 ml for regenerated cellulose (RC) films [13]. The PET/WCENFs film in the current study has a high retention volume for these EH with twice the initial concentration of EH solution compared to the commercial GMF, RC, PTFE, CA, and PP films reported by Han *et al*. [13]. Therefore, PET/WCENFs film can be used within this capacity for instant and concurrent removal of these EH solutes from wastewater. It can be a cheap and viable method by using waste CBs to make a WCENFs film for replacing the commercially available films for water treatment. The PET/WCENFs film can be an excellent substitute for the already available commercial films because this can be disposed of after several cycles, easily be detached, and replaced from a Swinnex film holder. Additionally, the WCENFs used as a film can be prepared by facile electrospinning technique, which is not costly.

3.7. Restrictions, further research, and application

This model study was limited to working with one concentration due to the restriction of solubility of four EH together, their detection, and quantification limits set on HPLC. Moreover, continuous long-term membrane testing on the cross and dead-end flow measurement under high pressures and flow rates, including membrane fouling, needs to be investigated. Furthermore, the influence of pH variation, interference of organic matter, ionic strength, temperature, the competing behavior of inorganic ions, varied concentrations of adsorbate and adsorbent dosage are some matters to be addressed in future research to help optimize the kinetics, determine isotherms and thermodynamic parameters. These works shall focus on actual reservoir samples to conclude the feasibility of this process for large-scale production.

3.8. Comparative study

Table 5 illustrates the type of fibers and particles used for the removal of hormones and pollutants from water. As can be seen, the WCENFs have a cumulative adsorption capacity of 2.14 mg/g, which is

Table 5. Comparison of adsorbents used for the specified water pollutants.

Adsorbents	Pollutant adsorption capacity [mg/g]					Reference
	E1	E2	E3	EE2	BPA	
MWCNTs	0.423	0.472	–	0.472	–	[60]
PA612	–	–	–	25.4	–	[47]
Darco AC	–	–	–	27.6	–	
Norit AC	–	–	–	10.4	–	
Un-anthracite	–	–	–	0.2147	0.1221	[68]
4 K anthracite	–	–	–	0.6209	0.1540	
PU Elastollan	0.801	0.592	0.382	0.736	–	[50]
PU 918	0.816	0.606	0.366	0.637	–	
CA	0.506	0.532	0.389	0.668	–	
PAN	0.396	0.370	0.397	0.343	–	
PES	0.442	0.487	0.363	0.591	–	
PA	0.331	0.543	0.485	0.611	–	
WCENFs	0.551	0.532	0.369	0.687	–	Present study

greater than most of the electrospun fibers (individual values are specified in Table 5) reported in the literature. Apart from that, the given particles (PA612, Darco AC, and Norit AC) have higher adsorption capacities than WCENFs due to their higher surface area based on the nature of those materials. Also, the individual adsorption capacities of WCENFs are firmly in compliance with those of electrospun CA fibers.

4. Conclusions

This study focused on concurrent removal of four EH (E1, E2, EE2, E3) to replicate real-time waste streams using WCENFs, recycling, and green approach. A one-step detection and concomitant quantification method based on HPLC was devised for these EH. It is noteworthy to mention that the WCENFs membrane could successfully remove all of these EH. The chemical composition of polymer, functional groups present, and structure of WCENFs played an essential role in the rapid adsorption process, which is elaborated in the adsorption mechanism. The strong affinity of WCENFs was found to be towards all EH due to abundant hydrogen bonding interactions. The highest percentage removal efficiencies from the batch adsorption were 64.3, 53.6, 52.7, and 34.6% for EE2, E1, E2, and E3, respectively. The total adsorption capacity obtained was 2.14 mg/g, and reported individual adsorption capacities of E1, E2, EE2, and E3 were found to be 0.551, 0.532, 0.687, and 0.369 mg/g, respectively. Based on the kinetic modeling results, the pseudo-first-order suits E3 and the pseudo-second-order model is suitable for E1, E2, and EE2. Therefore, both models are considered most appropriate due to their high regression coefficients than the other kinetic models. Desorption studies for the recovery of EH and reuse of submicron WCENFs was conducted and validated for four cycles using HPLC grade ethanol as the most suitable solvent. To summarize, the fabricated PET/WCENFs syringe film successfully responded to the retention time for these EH compared to the commercial CA syringe film. It also implies that recycled WCENFs can be considered a promising adsorbent for rapidly remediation of wastewater streams and possibly replacing the commercially available CA syringe film.

Acknowledgements

The authors gratefully acknowledge the financial support by the Ministry of Education, Youth, and Sports of the Czech Republic (grant no. RP/CPS/2020/002), the Internal Grant Agency of TBU in Zlin (grant no. IGA/CPS/2021/002). We would also like to acknowledge the Centre of Polymer Systems (CPS) situated at Tomas Bata University in Zlin, Czech Republic, to use the available research facilities to conduct this research work. Furthermore, the authors very much appreciate the assistance in laboratory equipment by Dr. Lenka Lovecka in CPS.

References

[1] Torkashvand J., Farzadkia M.: A systematic review on cigarette butt management as a hazardous waste and prevalent litter: Control and recycling. Environmental Science and Pollution Research, **26**, 11618–11630 (2019).
https://doi.org/10.1007/s11356-019-04250-x

[2] Shen F., Tian D., Yang G., Deng S., Shen F., He J., Zhu Y., Huang C., Hu J.: Deacetylation processing of waste cigarette butts for high-titer bioethanol production toward a clean recycling process. ACS Sustainable Chemistry and Engineering, **8**, 11253–11262 (2020). https://doi.org/10.1021/acssuschemeng.0c03979

[3] Rebischung F., Chabot L., Biaudet H., Pandard P.: Cigarette butts: A small but hazardous waste, according to european regulation. Waste Management, **82**, 9–14 (2018). https://doi.org/10.1016/j.wasman.2018.09.038

[4] Montalvão M. F., Chagas T. Q., da Silva Alvarez T. G., Mesak C., da Costa Araújo A. P., Gomes A. R., de Andrade Vieira J. E., Malafaia G.: How leachates from wasted cigarette butts influence aquatic life? A case study on freshwater mussel *Anodontites trapesial*i. Science of the Total Environment, **689**, 381–389 (2019). https://doi.org/10.1016/j.scitotenv.2019.06.385

[5] Benavente M. J., Caballero M. J. A., Silvero G., López-Coca I., Escobar V. G.: Cellulose acetate recovery from cigarette butts. Proceedings, **2**, 1447 (2019). https://doi.org/10.3390/proceedings2201447

[6] Hemamalini T., Karunakaran S. A., Siva Elango M. K., Senthil Ram T., Giri Dev V. R.: Regeneration of cellulose acetate nanofibrous mat from discarded cigarette butts. Indian Journal of Fibre and Textile Research, **44**, 248–252 (2019).

[7] Bilge S., Bakirhan N. K., Osman Donar Y., Sınağ A., Ozkan S. A.: Turning toxic cigarette butt waste into the sensor material for the sensitive determination of antihypertensive drug trandolapril from its dosage form and biological samples. Sensors and Actuators, B: Chemical, **296**, 126626 (2019). https://doi.org/10.1016/j.snb.2019.126626

[8] Alhokbany N. S., Naushad M., Kumar V., Al hatim S., Alshehri S. M., Ahamad T.: Self-nitrogen doped carbons aerogel derived from waste cigarette butts (cellulose acetate) for the adsorption of BPA: Kinetics and adsorption mechanisms. Journal of King Saud University – Science, **32**, 3351–3358 (2020). https://doi.org/10.1016/j.jksus.2020.09.021

[9] Schäfer A. I., Stelzl K., Faghih M., Sen Gupta S., Krishnadas K. R., Heißler S., Pradeep T.: Poly(ether sulfone) nanofibers impregnated with β-cyclodextrin for increased micropollutant removal from water. ACS Sustainable Chemistry and Engineering, **6**, 2942–2953 (2018). https://doi.org/10.1021/acssuschemeng.7b02214

[10] Luo Y., Guo W., Ngo H. H., Nghiem L. D., Hai F. I., Zhang J., Liang S., Wang X. C.: A review on the occurrence of micropollutants in the aquatic environment and their fate and removal during wastewater treatment. Science of the Total Environment, **473–474**, 619–641 (2014). https://doi.org/10.1016/j.scitotenv.2013.12.065

[11] Tijani J. O., Fatoba O. O., Petrik L. F.: A review of pharmaceuticals and endocrine-disrupting compounds: Sources, effects, removal, and detections. Water, Air, and Soil Pollution, **224**, 1770 (2013). https://doi.org/10.1007/s11270-013-1770-3

[12] Vymazal J., Březinová T., Koželuh M.: Occurrence and removal of estrogens, progesterone and testosterone in three constructed wetlands treating municipal sewage in the Czech Republic. Science of the Total Environment, **536**, 625–631 (2015). https://doi.org/10.1016/j.scitotenv.2015.07.077

[13] Han J., Qiu W., Gao W.: Adsorption of estrone in microfiltration membrane filters. Chemical Engineering Journal, **165**, 819–826 (2010). https://doi.org/10.1016/j.cej.2010.10.024

[14] Nghiem L. D., Schäfer A. I.: Adsorption and transport of trace contaminant estrone in NF/RO membranes. Environmental Engineering Science, **19**, 441–451 (2002). https://doi.org/10.1089/109287502320963427

[15] Solomon G. M., Schettler T.: Environment and health: 6. Endocrine disruption and potential human health implications. CMAJ, **163**, 1471–1476 (2000).

[16] Braga O., Smythe G. A., Schäfer A. I., Feitz A. J.: Fate of steroid estrogens in Australian inland and coastal wastewater treatment plants. Environmental Science and Technology, **39**, 3351–3358 (2005). https://doi.org/10.1021/es0501767

[17] Montes-Grajales D., Olivero-Verbel J.: EDCs databank: 3D-structure database of endocrine disrupting chemicals. Toxicology, **327**, 87–94 (2015). https://doi.org/10.1016/j.tox.2014.11.006

[18] Gyllenhammar I., Glynn A., Jönsson B. A. G., Lindh C. H., Darnerud P. O., Svensson K., Lignell S.: Diverging temporal trends of human exposure to bisphenols and plastizisers, such as phthalates, caused by substitution of legacy EDCs? Environmental Research, **153**, 48–54 (2017). https://doi.org/10.1016/j.envres.2016.11.012

[19] Sood S., Shekhar S., Santosh W.: Dimorphic placental stress: A repercussion of interaction between endocrine disrupting chemicals (EDCs) and fetal sex. Medical Hypotheses, **99**, 73–75 (2017). https://doi.org/10.1016/j.mehy.2017.01.002

[20] Luo L., Yang Y., Xiao M., Bian L., Yuan B., Liu Y., Jiang F., Pan X.: A novel biotemplated synthesis of TiO_2/wood charcoal composites for synergistic removal of bisphenol A by adsorption and photocatalytic degradation. Chemical Engineering Journal, **262**, 1275–1283 (2015). https://doi.org/10.1016/j.cej.2014.10.087

[21] Chen Y., Zhang Y., Luo L., Shi Y., Wang S., Li L., Long Y., Jiang F.: A novel templated synthesis of C/N-doped β-Bi_2O_3 nanosheets for synergistic rapid removal of 17α-ethynylestradiol by adsorption and photocatalytic degradation. Ceramics International, **44**, 2178–2185 (2018). https://doi.org/10.1016/j.ceramint.2017.10.173

[22] Semião A. J. C., Schäfer A. I.: Xenobiotics removal by membrane technology: An overview. in 'Xenobiotics in the urban water cycle' (eds.: Fatta-Kassinos D., Bester K., Kümmerer K.) Springer, Edinburgh, Vol. 16, 307–338 (2010).
https://doi.org/10.1007/978-90-481-3509-7_17

[23] Onesios K. M., Yu J. T., Bouwer E. J.: Biodegradation and removal of pharmaceuticals and personal care products in treatment systems: A review. Biodegradation, **20**, 441–466 (2009).
https://doi.org/10.1007/s10532-008-9237-8

[24] Pham T. T., Nguyen V. A., van der Bruggen B.: Pilot-scale evaluation of GAC adsorption using low-cost, high-performance materials for removal of pesticides and organic matter in drinking water production. Journal of Environmental Engineering, **139**, 958–965 (2013).
https://doi.org/10.1061/(asce)ee.1943-7870.0000704

[25] Ali H., Guler A. C., Masar M., Urbanek P., Urbanek M., Skoda D., Suly P., Machovsky M., Galusek D., Kuritka I.: Solid-state synthesis of direct *z*-scheme Cu_2O/WO_3 nanocomposites with enhanced visible-light photocatalytic performance. Catalysts, **11**, 293 (2021).
https://doi.org/10.3390/catal11020293

[26] Pendergast M. M., Hoek E. M. V.: A review of water treatment membrane nanotechnologies. Energy and Environmental Science, **4**, 1946–1971 (2011).
https://doi.org/10.1039/c0ee00541j

[27] Shannon M. A., Bohn P. W., Elimelech M., Georgiadis J. G., Marĩas B. J., Mayes A. M.: Science and technology for water purification in the coming decades. Nature, **452**, 301–310 (2008).
https://doi.org/10.1038/nature06599

[28] Kumar A. K., Mohan S. V.: Endocrine disruptive synthetic estrogen (17α-ethynylestradiol) removal from aqueous phase through batch and column sorption studies: Mechanistic and kinetic analysis. Desalination, **276**, 66–74 (2011).
https://doi.org/10.1016/j.desal.2011.03.022

[29] Kumar A. K., Mohan S. V., Sarma P. N.: Sorptive removal of endocrine-disruptive compound (estriol, E3) from aqueous phase by batch and column studies: Kinetic and mechanistic evaluation. Journal of Hazardous Materials, **164**, 820–828 (2009).
https://doi.org/10.1016/j.jhazmat.2008.08.075

[30] Pan B., Lin D., Mashayekhi H., Xing B.: Adsorption and hysteresis of bisphenol A and 17α-ethinyl estradiol on carbon nanomaterials. Environmental Science and Technology, **42**, 5480–5485 (2008).
https://doi.org/10.1021/es8001184

[31] Jin X., Hu J. Y., Tint M. L., Ong S. L., Biryulin Y., Polotskaya G.: Estrogenic compounds removal by fullerene-containing membranes. Desalination, **214**, 83–90 (2007).
https://doi.org/10.1016/j.desal.2006.10.019

[32] Kiran Kumar A., Venkata Mohan S.: Removal of natural and synthetic endocrine disrupting estrogens by multi-walled carbon nanotubes (MWCNT) as adsorbent: Kinetic and mechanistic evaluation. Separation and Purification Technology, **87**, 22–30 (2012).
https://doi.org/10.1016/j.seppur.2011.11.015

[33] Krupadam R. J., Sridevi P., Sakunthala S.: Removal of endocrine disrupting chemicals from contaminated industrial groundwater using chitin as a biosorbent. Journal of Chemical Technology and Biotechnology, **86**, 367–374 (2011).
https://doi.org/10.1002/jctb.2525

[34] Zhang Y., Zhou J. L.: Removal of estrone and 17β-estradiol from water by adsorption. Water Research, **39**, 3991–4003 (2005).
https://doi.org/10.1016/j.watres.2005.07.019

[35] Hristovski K. D., Nguyen H., Westerhoff P. K.: Removal of arsenate and 17α-ethinyl estradiol (EE2) by iron (hydr)oxide modified activated carbon fibers. Journal of Environmental Science and Health Part A: Toxic/Hazardous Substances and Environmental Engineering, **44**, 354–361 (2009).
https://doi.org/10.1080/10934520802659695

[36] Lu T., Liang H., Cao W., Deng Y., Qu Q., Ma W., Xiong R., Huang C.: Blow-spun nanofibrous composite self-cleaning membrane for enhanced purification of oily wastewater. Journal of Colloid and Interface Science, **608**, 2860–2869 (2022).
https://doi.org/10.1016/j.jcis.2021.11.017

[37] Ma W., Jiang Z., Lu T., Xiong R., Huang C.: Lightweight, elastic and superhydrophobic multifunctional nanofibrous aerogel for self-cleaning, oil/water separation and pressure sensing. Chemical Engineering Journal, **430**, 132989 (2022).
https://doi.org/10.1016/j.cej.2021.132989

[38] Wang J., Pan K., Giannelis E. P., Cao B.: Polyacrylonitrile/polyaniline core/shell nanofiber mat for removal of hexavalent chromium from aqueous solution: Mechanism and applications. RSC Advances, **3**, 8978–8987 (2013).
https://doi.org/10.1039/c3ra40616d

[39] Zhao J., Lu Z., He X., Zhang X., Li Q., Xia T., Zhang W., Lu C., Deng Y.: One-step fabrication of $Fe(OH)_3$@cellulose hollow nanofibers with superior capability for water purification. ACS Applied Materials and Interfaces, **9**, 25339–25349 (2017).
https://doi.org/10.1021/acsami.7b07038

[40] Kale S. M., Kirange P. M., Kale T. V., Kanu N. J., Gupta E., Chavan S. S., Vates U. K., Singh G. K.: Synthesis of ultrathin ZnO, nylon-6,6 and carbon nanofibers using electrospinning method for novel applications. MaterialsToday: Proceedings, **47**, 3186–3189 (2021).
https://doi.org/10.1016/j.matpr.2021.06.289

[41] Chigome S., Torto N.: A review of opportunities for electrospun nanofibers in analytical chemistry. Analytica Chimica Acta, **706**, 25–36 (2011).
https://doi.org/10.1016/j.aca.2011.08.021

[42] Chigome S., Darko G., Torto N.: Electrospun nanofibers as sorbent material for solid phase extraction. Analyst, **136**, 2879–2889 (2011).
https://doi.org/10.1039/c1an15228a

[43] Kanu N. J., Gupta E., Sutar V., Singh G. K., Vates U. K.: An insight into biofunctional curcumin/gelatin nanofibers. in Nanofibers – Synthesis, properties and applications' (ed.: Kumar B.) Intech Open, London, 1–22 (2021).
https://doi.org/10.5772/intechopen.97113

[44] Kanu N. J., Gupta E., Vates U. K., Singh G. K.: Electrospinning process parameters optimization for biofunctional curcumin/gelatin nanofibers. Materials Research Express, **7**, 035022 (2020).
https://doi.org/10.1088/2053-1591/ab7f60

[45] Arroyo F. D., Castro-Guerrero C. F., León-Silva U.: Thin films of cellulose acetate nanofibers from cigarette butt waste. Progress in Rubber, Plastics and Recycling Technology, **36**, 3–17 (2020).
https://doi.org/10.1177/1477760619895024

[46] Filep T., Szabó L., Kondor A. C., Jakab G., Szalai Z.: Evaluation of the effect of the intrinsic chemical properties of pharmaceutically active compounds (PhACs) on sorption behaviour in soils and goethite. Ecotoxicology and Environmental Safety, **215**, 112120 (2021).
https://doi.org/10.1016/j.ecoenv.2021.112120

[47] Han J., Qiu W., Cao Z., Hu J., Gao W.: Adsorption of ethinylestradiol (EE2) on polyamide 612: Molecular modeling and effects of water chemistry. Water Research, **47**, 2273–2284 (2013).
https://doi.org/10.1016/j.watres.2013.01.046

[48] Niavarani Z., Breite D., Prager A., Abel B., Schulze A.: Estradiol removal by adsorptive coating of a microfiltration membrane. Membranes, **11**, 99 (2021).
https://doi.org/10.3390/membranes11020099

[49] Wang M., Qu F., Jia R., Sun S., Li G., Liang H.: Preliminary study on the removal of steroidal estrogens using TiO_2-doped PVDF ultrafiltration membranes. Water, **8**, 134 (2016).
https://doi.org/10.3390/w8040134

[50] Yasir M., Šopík T., Lovecká L., Kimmer D., Sedlařík V.: The adsorption, kinetics, and interaction mechanisms of various types of estrogen on electrospun polymeric nanofiber membranes. Nanotechnology, **33**, 75702 (2021).
https://doi.org/10.1088/1361-6528/ac357b

[51] Cao W., Ma W., Lu T., Jiang Z., Xiong R., Huang C.: Multifunctional nanofibrous membranes with sunlight-driven self-cleaning performance for complex oily wastewater remediation. Journal of Colloid and Interface Science, **608**, 164–174 (2022).
https://doi.org/10.1016/j.jcis.2021.09.194

[52] Yasir M., Šopík T., Kimmer D., Sedlařík V.: Facile HPLC technique for simultaneous detection of estrogentic hormones in wastewater. in 'Proceedings of the 12th International Conference on Nanomaterials, Brno, Czech Republic' 272–276 (2021).
https://doi.org/10.37904/nanocon.2020.3710

[53] Qi F-F., Cao Y., Wang M., Rong F., Xu Q.: Nylon 6 electrospun nanofibers mat as effective sorbent for the removal of estrogens: Kinetic and thermodynamic studies. Nanoscale Research Letters, **9**, 353 (2014).
https://doi.org/10.1186/1556-276X-9-353

[54] Han J., Qiu W., Hu J., Gao W.: Chemisorption of estrone in nylon microfiltration membranes: Adsorption mechanism and potential use for estrone removal from water. Water Research, **46**, 873–881 (2012).
https://doi.org/10.1016/j.watres.2011.11.066

[55] Ma H., Burger C., Hsiao B. S., Chu B.: Nanofibrous microfiltration membrane based on cellulose nanowhiskers. Biomacromolecules, **13**, 180–186 (2012).
https://doi.org/10.1021/bm201421g

[56] Taha A. A., Wu Y-N., Wang H., Li F.: Preparation and application of functionalized cellulose acetate/silica composite nanofibrous membrane *via* electrospinning for Cr(VI) ion removal from aqueous solution. Journal of Environmental Management, **112**, 10–16 (2012).
https://doi.org/10.1016/j.jenvman.2012.05.031

[57] Mikaeili F., Gouma P. I.: Super water-repellent cellulose acetate mats. Scientific Reports, **8**, 12472 (2018).
https://doi.org/10.1038/s41598-018-30693-2

[58] Szewczyk P. K., Ura D. P., Metwally S., Knapczyk-Korczak J., Gajek M., Marzec M. M., Bernasik A., Stachewicz U.: Roughness and fiber fraction dominated wetting of electrospun fiber-based porous meshes. Polymers, **11**, 34 (2018).
https://doi.org/10.3390/polym11010034

[59] Schäfer A. I., Akanyeti I., Semião A. J. C.: Micropollutant sorption to membrane polymers: A review of mechanisms for estrogens. Advances in Colloid and Interface Science, **164**, 100–117 (2011).
https://doi.org/10.1016/j.cis.2010.09.006

[60] Al-Khateeb L. A., Obaid A. Y., Asiri N. A., Abdel Salam M.: Adsorption behavior of estrogenic compounds on carbon nanotubes from aqueous solutions: Kinetic and thermodynamic studies. Journal of Industrial and Engineering Chemistry, **20**, 916–924 (2014).
https://doi.org/10.1016/j.jiec.2013.06.023

[61] Ersali S., Hadadi V., Moradi O., Fakhri A.: Pseudo-second-order kinetic equations for modeling adsorption systems for removal of ammonium ions using multi-walled carbon nanotube. Fullerenes, Nanotubes and Carbon Nanostructures, **3**, 150527104639002 (2013).
https://doi.org/10.1080/1536383x.2013.787610

[62] Tian Y., Wu M., Liu R., Li Y., Wang D., Tan J., Wu R., Huang Y.: Electrospun membrane of cellulose acetate for heavy metal ion adsorption in water treatment. Carbohydrate Polymers, **83**, 743–748 (2011).
https://doi.org/10.1016/j.carbpol.2010.08.054

[63] Ho Y. S., McKay G.: Application of kinetic models to the sorption of copper(II) on to peat. Adsorption Science and Technology, **20**, 797–815 (2002).
https://doi.org/10.1260/026361702321104282

[64] Vazquez-Velez E., Lopez-Zarate L., Martinez-Valencia H.: Electrospinning of polyacrylonitrile nanofibers embedded with zerovalent iron and cerium oxide nanoparticles, as Cr(VI) adsorbents for water treatment. Journal of Applied Polymer Science, **137**, 48663 (2020). https://doi.org/10.1002/app.48663

[65] Porter J. J., Porter R. S.: Filtration studies of selected anionic dyes using asymmetric titanium dioxide membranes on porous stainless-steel tubes. Journal of Membrane Science, **101**, 67–81 (1995). https://doi.org/10.1016/0376-7388(94)00278-7

[66] Behera S. K., Kim H. W., Oh J-E., Park H-S.: Occurrence and removal of antibiotics, hormones and several other pharmaceuticals in wastewater treatment plants of the largest industrial city of Korea. Science of the Total Environment, **409**, 4351–4360 (2011). https://doi.org/10.1016/j.scitotenv.2011.07.015

[67] Nasir M., Subhan A., Prihandoko B., Lestariningsih T.: Nanostructure and property of electrospun SiO_2-cellulose acetate nanofiber composite by electrospinning. Energy Procedia, **107**, 227–231 (2017). https://doi.org/10.1016/j.egypro.2016.12.133

[68] He J., Zhou Q., Guo J., Fang F.: Characterization of potassium hydroxide modified anthracite particles and enhanced removal of 17α-ethinylestradiol and bisphenol A. Environmental Science and Pollution Research, **25**, 22224–22235 (2018). https://doi.org/10.1007/s11356-018-2287-5